Deciphering the combinatorial expression pattern and genetic regulatory mechanisms of Beats and Sides in the olfactory circuits of *Drosophila*

Qichen Duan[1], Sumie Okuwa[1], Rachel Estrella[1], Chun Yeung[1], Yu-Chieh David Chen[2, 4], Laura Quintana Rio[3], Khanh M. Vien[1], Pelin C. Volkan[1, #]

1. Department of Biology, Duke University, Durham, NC 27708, USA
2. Department of Biology, New York University, New York, NY 10003, USA
3. Department of Biochemistry and Molecular Biophysics, Columbia University, New York, NY 10027, USA
4. Current Address: Department of Biology, Temple University, Philadelphia, PA 19122, USA.

Correspondence: pelin.volkan@duke.edu

Abstract

Over the past decades, many critical molecular players have been uncovered to control distinct steps in olfactory circuit assembly in Drosophila. Among these, multi-member gene families of cell surface proteins are of interest because they can act as neuron-specific identification/recognition tags in combinations and contribute to circuit assembly in complex brains through their heterophilic or homophilic interactions. Recently, a multi-protein interactome has been described between the Beat and Side families of IgSF proteins. Here, we use the publicly available single-cell RNA-seq datasets and newly generated gene trap transgenic driver lines to probe the *in vivo* spatial expression pattern of the *beat/side* gene families in odorant receptor neurons (ORNs) and their synaptic target projection neurons (PNs). Our results revealed that each ORN and its synaptic target PN class expresses a class-specific combination of *beat/side* genes, hierarchically regulated by lineage-specific genetic programs. Though ORNs or PNs from closer lineages tend to possess more similar *beat/side* profiles, we also found many examples of divergence from this pattern among closely related ORNs and closely related PNs. To explore whether the class-specific combination of *beats/sides* defines ORN-PN matching specificity, we perturbed presynaptic *beat-IIa* and postsynaptic *side-IV* in two ORN-PN partners. However, disruption of Beat-IIa-Side-IV interaction did not produce any significant mistargeting in these two examined glomeruli. Though without affecting general glomerular targeting, knockdown of *side* in ORNs leads to the reduction of synaptic development. Interestingly, we found conserved expression patterns of *beat/side* orthologs across ORNs in ants and mosquitoes, indicating the shared regulatory strategies specifying the expression of these duplicated paralogs in insect evolution. Overall, this comprehensive analysis of expression patterns lays a foundation for in-depth functional investigations into how Beat/Side combinatorial expression contributes to the olfactory circuit assembly.

Key words

Beaten path, Sidestep, olfactory circuit, Drosophila, neural development

Introduction

The *Drosophila* olfactory system provides an excellent model for understanding the genetic basis of the neuronal class-specific circuit organization and assembly. The first-order sensory neurons in the circuit are olfactory receptor neurons (ORNs), which are housed in the peripheral sensilla covering the antennae (Barish and Volkan, 2015; Brochtrup and Hummel, 2011; Hong and Luo, 2014; Jefferis and Hummel, 2006; Rodrigues and Hummel, 2008). Each ORN typically expresses only a single identity-defining olfactory receptor (OR) gene or a unique combination of up to three OR genes (Barish and Volkan, 2015). The cell bodies of ORNs expressing the same OR genes, thus of the same class, are dispersed across the antenna. Yet, their axons converge onto a single, uniquely positioned class-specific glomerulus in the antennal lobe, where they synapse with the second-order projection neurons (PNs) (Barish and Volkan, 2015; Hong and Luo, 2014). ORNs are thus defined by their OR expression and glomerular target identity, comprising ~60 classes (Task et al., 2022). PNs, born from distinct neuroblast lineages surrounding antennal lobes, are also defined by their unique dendritic targeting of the dedicated glomeruli. At the same time, their axons extend to other higher brain regions, mushroom bodies, and lateral horns, which integrate the odor signal with other sensory cues and internal states to guide the animals' behaviors (Hong and Luo, 2014; Jefferis et al., 2001; Li et al., 2018; Yu et al., 2010). Importantly, within the antennal lobe, ORNs and PNs form a one-to-one match in the class-specific glomerulus. This precisely controlled organization brings many interesting questions. How are these neurons born? What molecules mediate the communication between the neurons of the same class, different classes, or pre- and post-synaptic partners? How do these neurons acquire the necessary cell surface signaling to mediate these interactions that eventually ensure the formation of this stereotyped glomerular map? As this one-to-one structure maintains over evolution from insects to mammals (Imai et al., 2010), the easy and genetically tractable *Drosophila* is a great platform to determine the lineage-specific and combinatorial expression of cell surface proteins, their establishment, function, and evolution.

Many molecular players have been identified to participate in organizing the *Drosophila* olfactory circuits, ranging from the critical regulatory hubs at the top of the developmental hierarchy, like transcription factors instructing the lineage and/or the expression of a broad range of cell surface molecules (CSMs) (Komiyama et al., 2004; Komiyama et al., 2003; Li et al., 2020a; Tichy et al., 2008; Xie et al., 2022), to the executors at the bottom of the hierarchy, which are critical CSMs themselves. These include many members of large protein families, like leucine-rich repeat superfamily members Toll-6/Toll-7 (Ward et al., 2015), Fili (Li et al., 2025; Xie et al., 2019), and Capricious (Hong et al., 2009); Teneurins Ten-a and Ten-m (Hong et al., 2012; Mosca and Luo, 2014); Cadherin superfamily members Ncad (Hummel and Zipursky, 2004; Zhu and Luo, 2004), Flamingo (Arguello et al., 2021), and Fat2 (Kug) (Vien et al., 2023); Immunoglobulin Super Family (IgSF) members Dscam with extremely diverse isoform repertoire (Goyal et al., 2019; Hattori et al., 2007; Hummel et al., 2003; Zhu et al., 2006) and DIPs/Dprs, which consist of multiple paralogs (Barish et al., 2018). Our previous work showed that class-specific combinatorial expression of DIPs/Dprs organizes ORN axons within glomeruli (Barish et al., 2018). DIPs/Dprs are of particular interest because they form two multi-member subfamilies (11 DIPs and 21 Dprs), bind one another (Dprs to DIPs) primarily through heterophilic interactions, and exhibit striking cell-type-specific expression (Brovero et al., 2021; Carrillo et al., 2015; Cheng et al., 2019a; Cheng et al., 2019b;

Cosmanescu et al., 2018; Özkan et al., 2013; Wang et al., 2022). Besides the olfactory system, several trans-synaptically interacting DIPs and Dprs have been shown to control synapse selectivity and formation in the visual circuits and neuromuscular junction (Ashley et al., 2019; Carrillo et al., 2015; Courgeon and Desplan, 2019; Dombrovski et al., 2025; Menon et al., 2019; Tan et al., 2015; Venkatasubramanian et al., 2019; Xu et al., 2019; Xu et al., 2022; Xu et al., 2018).

There are around 130 IgSF-encoding genes in the Drosophila genome (Sanes and Zipursky, 2020). In addition to well-characterized DIPs/Dprs comprised of 32 members, another two families, the Beaten path (Beat) family (14 paralogs) and Sidestep (Side) family (eight paralogs) proteins (Figure 1A), are less studied. They share many features with DIPs/Dprs. They also belong to IgSF, with two or five extracellular Ig domains mediating adhesion (Figure 1B), and form a heterophilic interaction network (Figure 1A) (Li et al., 2017b; Özkan et al., 2013). Beats/Sides have been shown to control the neuromuscular junction formation in both larval and adult motor systems (de Jong et al., 2005; Fambrough and Goodman, 1996; Heymann et al., 2022; Kinold et al., 2021; Kinold et al., 2018; Pipes et al., 2001; Siebert et al., 2009; Sink et al., 2001). Very recently, studies have begun to reveal their roles in synaptic specificity and induction to assemble the adult visual system (Carrier et al., 2025; Dombrovski et al., 2025; Osaka et al., 2024; Yoo et al., 2023). However, little is known about whether and how they contribute to the olfactory circuit organization. We observed that the expression levels of *beats/sides* in antennal tissues increase over development, and most of them tend to have higher transcriptional levels in the latter half of the pupal stage, from 40h after puparium formation (APF) throughout adulthood (Figure S2A), during which the stereotyped glomerular map is being formed. Given their protein properties and known roles in neural development, we sought to illustrate the *beats/sides*' expression patterns and test their functions in building the *Drosophila* olfactory circuit.

In this study, we systematically characterized the expression pattern of *beat/side* family genes in both ORNs and PNs at single-cell and single-class levels. By analyzing the previously published single-cell RNA-seq datasets and genetically probing the native expression with *MiMIC*-based *beat/side* gene trap *GAL4* lines, we revealed that each ORN or PN class expresses a unique combination of *beats/sides*, and this *beat/side* profile is likely regulated by the lineage-specific genetic programs in a hierarchical manner. We also tested the functional relevance of one interacting pair, Beat-IIa and Side-IV, based on their matching expression pattern in partner ORNs and PNs. However, perturbation of either one pre- or post-synaptically did not result in apparent glomerular mistargeting. Nonetheless, we found pervasive ORN synapse defects when the *side* was knocked down in ORNs, suggesting its possible role in synaptic development. Interestingly, we found analogous expression principles for *beat/side* orthologs across ORNs in mosquitoes and ants, indicating the shared strategies across evolution for circuit assembly through lineage-specific regulation of cell surface protein combinations, particularly by coordinating the expression of multiple duplicated paralogs. Overall, our study reveals the combinatorial expression pattern and functional role that Beat/Side proteins play in olfactory circuit assembly and synaptic development.

Results

Genetically probing the *beat/side* expression *in vivo* by a collection of *MiMIC*-based gene trap driver lines

Recently, efforts to profile the transcriptional landscape of each cell across the whole fruit fly body have provided a valuable resource to examine the gene expression patterns in the cell types of interest. However, in the olfactory system, single-cell RNA-seq has only captured a limited portion of ORN or PN classes, leaving the transcriptome of many other ORN and PN classes unknown. To fully reveal the *beat/side* combinatorial profile, we used a *MiMIC*-based gene trap approach to generate a collection of transgenic *beat/side*-specific *GAL4* driver lines (Diao et al., 2015; Venken et al., 2011). By swapping the *GAL4* construct into 5' UTR-located *MiMIC* sites or the in-frame *T2A-GAL4* construct into introns between two coding exons, we could make GAL4 hijack the expression of the host gene (Figure 1C and Materials and Methods). We then obtained *GAL4* driver lines for 13 of the 14 *beat* members and seven of the eight *side* members, except *beat-Vb* and *side-VII* (Figure 1D, E). Notably, *beat/side* genes generally have one to four annotated isoforms, and our *beat/side-MiMIC GAL4* collection is expected to trap all isoforms of each gene except *beat-IIb*, of which the *GAL4* only captures the expression of one of two isoforms (Figure 1E). This near-complete driver line collection reveals the remarkable enrichment of *beat/side* expression in neurons, from larval, pupal, to adult stages, in both peripheral and central nervous systems (Figure 1D; Figure S1). At the gross brain level, *beats/sides* are differentially expressed across different brain regions, including the antennal lobe, central complex, mushroom body, etc. (Figure 1D). This driver collection thus provides a valuable toolkit to study *beat/side* functions in diverse neuronal contexts in the olfactory circuits and beyond. Next, we used intersectional genetic strategies to restrict the reporter expression to ORNs or PNs, which allowed us to map the *beat/side* expression across glomeruli innervated by ORNs or PNs, respectively.

A glomerular map of *beat/side* expression in ORNs

Our antennal bulk RNA-seq through pupal development shows that *beats/sides* are generally expressed at higher levels at later stages of glomerular formation, reaching the adult levels by mid-pupal stages (Figure S2A). To delineate the *beat/side* expression in each ORN class, we examined the publicly available single-ORN RNA-seq datasets from three distinct developmental stages: 24h APF (early pupal stage), 42-48h APF (mid-pupal stage), and adulthood (Li et al., 2020a; McLaughlin et al., 2021). At 24h APF, ORN axons have arrived at the antennal lobes and chosen a medial versus lateral antennal lobe trajectory, which positions them en route to their future glomerular regions. By the mid-pupal stage, the glomerular targeting is almost completed, and ORNs start forming synapses with their matching postsynaptic PNs. By the beginning of the adult stage, a stereotypical and discrete glomerular map has formed, and all glomeruli are now discernible. We visualized these datasets in bubble plots showing the fraction of positive cells and the mean expression of genes of interest of each ORN class (Figure S2B). This reveals that each ORN class possesses a unique signature of *beat/side* combinations throughout the developmental stages (Figure S2B). Combining bulk antennal RNA-seq and ORN single-cell RNA-seq results, we found that *sides* are generally expressed at higher levels in ORNs than *beats* (Figures S2A, B). Some *beats*, including *beat-Va*, *beat-Vb*, and *beat-Vc*, are barely expressed in any cell types within the

antenna, whereas *side-VIII* appears to be predominantly expressed in non-neuronal cells of the antenna but not in ORNs (Figure S2A, B).

As many ORN classes are not captured in the single-cell RNA-seq datasets, we used the *MiMIC-GAL4* lines to probe the ORN expression of different *beats/sides in vivo* in 3-5-day-old adult brains as the proxy of their developmental expression. We leveraged the *eyeless*-driven FLP recombinase to excise the *STOP* cassette from *UAS-FRT-STOP-FRT-mCD8.GFP*, such that membrane-localized GFP expression by *beat/side-GAL4* can be restricted to ORNs. This way, we can label any glomeruli innervated by ORNs expressing each *beat/side* while excluding the signal from post-synaptic PNs, where *eyeless* has no expression. We generated a near-complete glomerular *beat/side* expression map across all ORN classes (Figure 2A). Consistent with bulk and single-cell RNA-seq, *beat-Ic*, *beat-Va*, and *side-VIII* are not expressed in any ORN classes. Some family members, like *beat-Ib*, *beat-VI*, and *side-IV,* are only sparsely expressed in very few ORN classes (Figure 2A). On the other hand, other *beats/sides* are expressed in a much broader pattern, though at varying levels among different ORN classes (Figure 2A).

Based on the GAL4 labeling patterns, we binarized the expression of all examined *beat* and *side* genes, as positive (value = 1) or negative (value = 0) for each gene in each ORN target glomerulus. We summarized the results and hierarchically clustered the genes by their expression pattern and ORN classes by their *beat/side*-expression profile, as shown in Figure 2B. We observed three types of gene expression patterns for *beat* and *side* genes across ORN classes: (1) broadly expressed, (2) expressed at a restricted pattern, or (3) not expressed (Figure 2B). More interestingly, ORN classes from the same lineage tend to be clustered based on the combinatorial *beat/side* expression (Figure 2B). This suggests a lineage-specific mechanism in patterning the ORN class-specific combinatorial expression of *beats/sides*. We decided to investigate this in further detail.

Lineage-regulated genetic programs specify the combinatorial expression of *beats/sides* in ORNs

ORNs differentiate from precursor cells via a multi-step hierarchical genetic program (Barish and Volkan, 2015; Li et al., 2018). Early larval and pupal patterning factors first prepattern antennal imaginal discs (Royet and Finkelstein, 1997), followed by the sensillar type assignment by critical transcription factors, including Lozenge (Lz), Atonal, and Amos (Figure S2C) (Goulding et al., 2000; Gupta et al., 1998; Gupta and Rodrigues, 1997; zur Lage et al., 2003). We first examined the bulk antennal RNA-seq datasets profiling the transcriptional changes in mutants of *amos* (lacking trichoid and basiconic ORNs) or *atonal* (lacking coeloconic ORNs) (Menuz et al., 2014; Mohapatra and Menuz, 2019). We indeed found a couple of *beats/sides* that are downregulated in *atonal* and *amos* mutant antennae (Figure S2D), suggesting these *beats/sides* are enriched in the cells housed in Amos/Atonal-specified sensillar types. A few genes are also upregulated in *amos* and *atonal* mutants (Figure S2D). These *beat* and *side* genes are either transcriptionally upregulated or are now enriched in the mutants due to changes in ORN ratios.

Upon sensillar type selection, sensillar subtype fates are further specified by an additional set of transcription factors like Rotund (Rn), Dachshund (Dac), and Engrailed (En) (Figure S2C) (Barish and Volkan, 2015; Blagburn, 2008; Li et al., 2016; Li et al., 2013; Song et al., 2012).

Finally, within each sensillar subtype (or sensillum), one multipotent precursor cell undergoes several sequential asymmetric divisions that eventually produce one to four different ORNs expressing distinct ORs and projecting to distinct glomeruli and four non-neuronal supporting cells (Barish and Volkan, 2015; Li et al., 2018). This step is achieved by iterative recruitment of Notch signaling bifurcating cell fates, coupled with other mechanisms like epigenetic modifiers and late transcription factors (Barish and Volkan, 2015; Chai et al., 2019; Endo et al., 2007) (Figure S2C). We here present a simplified decision tree to illustrate the kinships between ORNs and to compare *beat/side* combinations based on lineage relationships (Figure S2C): ORNs mapped to the same class, defined as “within ORN class”; ORNs of different classes but housed in the same sensillar subtype, described as “within sensillar subtype”; ORNs from different sensillar subtypes but belonging to the same sensillar type, namely, “within sensillar type”; and the furthest kinship, ORNs housed in distinct sensillar types, i.e., “between sensillar types”. We compared the similarity of *beat/side* combinatorial expression between cells falling into these ORN kinship categories to obtain insights into the developmental regulation of *beat/side* expression.

Firstly, based on our gene-ORN class expression matrix derived from the genetic labeling data (Figure 2B), we calculated the similarity (Pearson’s correlation) of the *beat/side* expression vector between each ORN class pair, and found significantly higher similarity between ORN classes belonging to the same sensillar types than those from different sensillar types (Figure 2C). In contrast, this pattern is not observed from the randomized control, where we shuffled the ORN class identity with the expression vector (Figure 2D). Additionally, we found that this difference also holds for the single-cell RNA-seq datasets. By calculating the similarity (measured by Spearman’s correlation) according to gene expression between each single ORN, we found that, as expected, ORNs mapped to the same class display the highest pairwise similarity of *beat/side* profile in all stages (Figure 2E; Figure S2E). Moreover, ORNs within the same sensillar type appear to possess more similar *beat/side* profiles than ORNs from different sensillar types, in contrast to the shuffled control (Figure 2E, F), supporting that the lineage-intrinsic mechanisms set the *beat/side* expression.

However, we found that *beat/side* combinatorial expression tends to diverge between ORNs housed in the same sensillar subtype (Figure S2E). We observed even lower pairwise similarity according to the *beat/side* expression between these cells than between cells from different sensillar subtypes but sharing the identical sensillar type (Figure S2E). This observation stands true for all three stages (Figure S2E). In contrast, at 24h APF and mid-pupal stage, the similarity of the pan-CSM profile and the whole transcriptome linearly increases with closer kinship (Figure S2E). It suggests that the overall transcriptional profile and the cell surface gene expression patterns are primarily set by lineage-specific factors, such that cells with closer kinship tend to have more similar transcriptomic profiles and overall cell surface codes. Furthermore, *beats/sides* expression adds new levels of complexity to cell surface signals, potentially diversifying ORN-specific glomerular decisions, particularly among the most developmentally related ORNs in the same sensillar subtype. Interestingly, at the adult stage, this divergence also exists for overall CSM and cell-specific transcriptional profiles (Figure S2E). These results suggest that at the end of development, ORNs with the closest kinship may have acquired broader transcriptional variance, which may support the establishment of discrete glomerular maps necessary for olfactory transduction, odor discrimination, and processing to drive odor-guided behaviors.

While the single-cell RNA-seq-based analysis only reflects the trend for the limited cell types captured in that dataset, our genetic labeling-based comprehensive analysis of *beat/side* across all ORN classes reveals the existence of both convergence and divergence: ORNs from the same sensillar subtype exhibit binary *beat/side* similarity: they could be clustered together, suggesting their shared *beat/side* combinatorial expression; they could also be segregated, indicating the divergence of *beat/side* profile from genetically very close ORNs (Figure 2B). We therefore propose a model: in some sensillar subtypes, at the step of ORN terminal selection, *beat/side* combinatorial expression is diversified from a putative initial lineage-specific "template" to ensure the closely related ORNs gain more variation in these cell surface molecular repertoire, whereas in some sensillar subtypes, *beat/side* profile is pre-specified and these closely related ORNs show similar *beat/side* combinations.

Collectively, our thorough characterization of *beat/side* expression from both single-cell RNA-seq and gene trap *GAL4* intersectional labeling suggests that Beats/Sides could be the cell surface "executors" underlying the hierarchical genetic programs that specify the ORN fate, likely participating in fine-tuning the ORN wiring.

A glomerular map of *beat/side* expression in PNs

ORNs synapse with dedicated PNs within each glomerulus to assemble the olfactory circuit, and Beats/Sides are involved in synaptogenesis (Osaka et al., 2024; Yoo et al., 2023). We also need to survey the *beat/side* expression on the PN side, which may inform whether Beats/Sides could function trans-synaptically to mediate ORN-PN matching. We started with the bulk PN RNA-seq (Li et al., 2020b) from the FACS-sorted PNs at 36h APF and adult stage. In general, *beats/sides* appear to be expressed at commensurate levels between these two time points (Figure S3A). Next, we mined the published single-cell RNA-seq data (Li et al., 2017b; Xie et al., 2021) for developing PNs to gain insights into the PN type-specific expression of *beats/sides*. This dataset captured PNs at 0h APF, 24h APF, 48h APF (mid-pupal), and the adult stage. Some PNs are born embryonically and are part of the larval olfactory circuit (Jefferis et al., 2001; Lin et al., 2012; Marin et al., 2005; Yu et al., 2010). At the beginning of the pupal stage, these PNs first prune their terminal axons and dendrites and re-extend their neurites to be integrated into the adult olfactory circuit following other larvally born PNs (Marin et al., 2005). From 0h to 24h APF, PNs project their axons to the mushroom body and lateral horn and their dendrites to the antennal lobes. PNs' dendrites create a prototypical glomerular map before ORN axons arrive in the antennal lobes at around 24h APF. Thereafter, PNs begin to match their presynaptic ORN partners. And starting from the mid-pupal stage, they build synapses, refine the discrete glomerular organization, and finally mature the olfactory circuit by the end of the pupal stage (Jefferis et al., 2001). In terms of PN class-specific expression of *beats/side*s at different time windows, we found: (1) *beats/sides* are enriched at 24h APF and thereafter, while expressed at minor levels at the beginning of metamorphosis (Figure S3B); (2) compared with ORNs, *beats/sides* are generally expressed in a broader pattern, and all *beats/sides* are expressed in PNs while some *beats* and *side-VIII* are undetectable in ORNs (Figures S2B, S3B). Suppose Beats/Side mediate adhesion between ORNs and PNs; this observation raises a hypothetical model where broadly and less specifically located postsynaptic surface "locks" are matched by sparsely and more specifically distributed presynaptic surface "keys".

307 Next, we used these *GAL4* lines to drive the GFP reporter expression in postsynaptic PNs by
308 removing the *STOP* cassette from *UAS-FRT-STOP-FRT-mCD8.GFP* with the PN-specific
309 *GH146-flippase*. We found generally broader expression of *beats/sides* across PN-labeled
310 glomeruli, with a few sparsely distributed ones, like *beat-Ic* and *side-IV* (Figure 3A). We then
311 summarized the binary expression of all *beats/sides* examined across all glomeruli identified
312 (Figure 3B). Hierarchical clustering of PN types according to their *beat/side* expression shows,
313 in general, a correlation between *beat/side* combination and their PN lineages (Figure 3B). We
314 therefore further investigated this.

315

316 **Lineage-regulated genetic programs specify the combinatorial expression of**
317 ***beats/sides* in PNs**

318 PN fates are specified separately from ORNs by a sequential genetic program from three
319 distinct neuroblast lineages (Figure S3C) (Jefferis et al., 2001; Li et al., 2018). A common
320 neuroblast sequentially produces one ganglion mother cell and a self-renewed neuroblast. The
321 ganglion mother cell further divides into one terminal PN, which innervates a dedicated
322 glomerulus, and another daughter cell, which undergoes cell death (Lin et al., 2012; Lin et al.,
323 2010). The younger neuroblast continues this process. Thus, different PN classes are born in a
324 sequentially stereotyped order (Jefferis et al., 2001; Lin et al., 2012; Yu et al., 2010). Based on
325 this, we defined the relationship between PNs into three categories: (1) PNs from the same
326 lineage targeting the same glomerulus, (2) PNs from the same lineage targeting different
327 glomeruli, and (3) PNs from different lineages targeting different glomeruli.

328 We again asked whether the *beat/side* profile similarity between PN classes is based on their
329 developmental kinship. Calculating the PN class-specific *beat/side* expression similarity based
330 on the *GAL4* labeling expression matrix showed higher similarity between PN classes of the
331 same lineage than of different lineages (Figure 3C, D). Similarity analysis for *beat/side*
332 expression in the single-PN RNA-seq datasets also confirmed these observations (Figure 3E,
333 F; Figure S3D). In the same lineage, as expected, PNs targeting the same glomeruli also have
334 more similar *beat/side* expression than PNs targeting different glomeruli (Figure S3D). This is
335 also true for the expression of CSMs and the cellular transcriptional profiles at all four stages
336 (Figure S3D). This suggests that, as part of their cell surface repertoire, the *beat/side* profiles
337 in PNs are primarily set by the lineage and PN class-specific genetic mechanisms.

338 As PNs in each lineage are born in a stereotyped order, we also examined whether PN birth
339 order determines its *beat/side* profile. We focused on the adPN lineage and calculated the
340 correlation between each PN pair. We plotted their *beat/side* profile and sorted the PN classes
341 in this lineage based on the reported birth order (Figure 3G). We also plotted the Pearson's
342 correlation coefficient between each pair of PN classes (Figure 3H). We found that the early-
343 born PNs have more divergent *beat/side* profiles while later-born PNs gradually obtain a
344 shared Beat/Side combinatorial "template" which gets less complex as new PN fates are
345 generated (Figure 3G, H). This trend indicates that PN precursor-specific factors set the
346 *beat/side* expression potential of daughter PNs and undergo a temporal fate specification
347 along with the birth sequence of PNs. It is also interesting that, similar to ORNs (Figure 2B, C),
348 closely related PNs can possess shared or divergent *beat/side* combinatorial expression,
349 suggesting that different intrinsic genetic programs may be present in different precursor cells
350 to control the opposing *beat/side* expression similarity in their daughter cells.

351

352 **Beats/Sides form a robust molecular interaction network between ORN and PN partners**

353 The first identified Beat-Ia and Side pair act trans-synaptically to promote synapse formation at
354 the neuromuscular junction (Fambrough and Goodman, 1996; Kinold et al., 2021; Kinold et al.,
355 2018; Siebert et al., 2009; Sink et al., 2001). Recent work also identified additional Beat-Side
356 interactions, including Side-IV and Beat-IIa/b, mediating neuronal recognition, connection
357 specificity, and synaptogenesis in the fly visual system (Osaka et al., 2024; Yoo et al., 2023).
358 We, therefore, hypothesized that Beat and Side interactions between ORNs and PNs can also
359 regulate the synaptic matching. Guided by the known Beat-Side interactions based on the *in*
360 *vitro* biochemical assays, we examined the *beat/side* expression between partner ORN and
361 PN targeting the same glomerulus (Figures 1A, 4A). This analysis revealed a putative
362 Beat/Side-mediated interactome between ORNs and PNs, which is promiscuous, redundant,
363 and complex.

364 While several putative Beat-Side interactions exist between partner ORN and PN classes, we
365 found one elegant and straightforward case: presynaptic Beat-IIa and postsynaptic Side-IV.
366 *beat-IIa* is expressed in just a few ORN classes, including Or42b ORNs targeting one posterior
367 glomerulus DM1 and Or92a ORNs targeting one anterior glomerulus VA2 (Figure 4B). In
368 parallel, *side-IV* expression is restricted in PNs, including PNs projecting to DM1 and VA2
369 glomeruli (Figure 4C). Next, we tested whether perturbing *beat-IIa* expression in ORNs or *side-*
370 *IV* expression in PNs results in glomerular targeting defects. To do this, we used a pan-ORN
371 driver, *peb-GAL4,* to knock down *beat-IIa* in all ORNs while labeling Or42b ORNs or Or92a
372 ORNs as a readout of glomerular targeting. However, we did not observe any gross phenotype
373 in glomerular integrity, morphology, position, or ectopic mistargeting (Figure 4D, E). We also
374 used a PN-specific driver, *GH146-GAL4,* to express *side-IV RNAi* and test if Or42b or Or92a
375 ORNs target their glomeruli normally. Again, we found no visible differences between
376 knockdowns and controls (Figure 4F, G). These results suggest that either Beat-IIa/Side-IV
377 interaction in matching ORNs and PNs is unnecessary for glomerular targeting or is
378 compensated by other Beat and Side proteins with redundant functions expressed in the same
379 neurons.

380 Indeed, the combinatorial *beat/side* codes can distinguish ORNs targeting DM1 or VA2
381 glomeruli from ORNs innervating the neighboring glomeruli (Figure 4H), such that removing
382 *beat-IIa* in ORNs doesn't ambiguate the CSM repertoire and still preserves a level of diversity
383 among the local axon fibers in a glomerular neighborhood. Similarly, PNs targeting DM1 or
384 VA2 also harness this robust combinatorial "barcode", and deleting *side-IV* in PNs may not
385 abolish the dendritic diversity in the glomerular neighborhood (Figure 4I). To test for general
386 defects in glomerular organization, we also conducted a pan-ORN driver *peb-GAL4* driven
387 *UAS-RNAi* screening against *beat* and *side* genes that are expressed in ORNs (Figure S4A).
388 This screen revealed mild defects in the VA1v glomerulus targeted by Or47b ORNs by
389 knockdown of *beat-IIb, beat-IIIa/b/c,* and *side-III*, and a low-penetrance phenotype of split DM3
390 glomerulus targeted by Or47a ORNs (Figure S4A, B). However, additional controls showed
391 that the VA1v phenotypes of *beat-IIIa/b/c* perturbation appeared to arise from the transgenic
392 background that sensitizes the VA1v glomerular disorganization (Duan et al., 2023)(Figure
393 S4C). These negative results might be because the Beat/Side combinatorial expression can
394 theoretically act as a robust cell surface recognition code for each ORN or PN class, given its
395 error-tolerance feature.

Given the lack of glomerular targeting defects, we next asked whether *beat* and *side* genes have roles in regulating synapse development and maintenance within glomeruli. For this, we used a previously generated transgenic reporter, *UAS-SynLight*, which expresses the presynaptic active zone marker, Bruchpilot-Short (sBRP), and the neurite membrane marker mCD8.GFP in the same transcript (Aimino et al., 2023). We expressed this transgene in ORNs to label and quantify the synaptic density in the antennal lobes while doing perturbation in ORNs. We calculated the ratio of the mean fluorescence intensity of RFP and GFP in the antennal lobe as a proxy of synaptic density (Figure S5A). This way normalizes the potential variability in transcription levels, imaging conditions, or neuron size across groups. As inhibiting neural activity has been reported to decrease synapse numbers, we first silenced ORN neuronal activity by overexpressing the mutant *shaker* channel EKO. We observed synaptic density reduction globally in the antennal lobe, compared with the control group where an inactive variant of tetanus toxin light-chain (TNT-) was introduced instead (Figure S5B, C). This confirmed the feasibility of using this transgenic reporter to measure synapses and the effect of neural activity on synaptogenesis.

We next used the pan-ORN *peb-GAL4* to knock down *beats/sides* that are expressed in ORNs and have known interacting partners. We also knocked down *side-VIII*, which is not expressed in ORNs, to serve as a presumable negative control (Figure 2A, B; Figure S2B). We found a pervasive synaptic reduction in *side* knockdowns compared to the control *RNAi,* but not *side-VIII* knockdowns (Figure 4J; Figure S5D, E). In contrast, knockdown of sparsely expressed genes, including *beat-IIa/b* and *side-IV*, didn't lead to detectable differences from controls (Figure 4A; Figure S5D, E). Additionally, knockdown of other broadly expressed ones, including *beat-Ia*, *side-II, side-III*, and *side-VI*, also didn't cause significant changes in synaptic density of ORNs, except *side-VII*, which increased the overall synaptic density in the antennal lobe (Figure 4A; Figure S5D, E). The discrepancy of loss-of-function effects between *side* and other broadly expressed ones could be due to the biochemical property of Side protein, which interacts with four Beat partners, more than any other Side family members (Figure 1A). It is likely that a lack of Side leads to a more substantial reduction in trans-synaptic adhesion than the lack of other Side proteins (Figure 4A). As opposed to *side* with potential functions in synapse induction, *side-VII* might play a role in inhibiting synapse formation. Though we were unable to map the *side-VII* expression pattern in the antennal lobe as the gene trap driver is unavailable, the single-cell RNA-seq datasets show that *side-VII* appears to be broadly expressed across ORN classes and may interact with its cognate partner Beat-IV, which is also broadly expressed across PN classes as well as ORN classes (Figures 2B, 3B; Figures S2B, S3B). Thus, Side-VII might inhibit synapse formation through either *trans* interaction with post-synaptic Beat-IV or *cis* binding with Beat-IV on the same membrane. Overall, our results suggest the bidirectional regulatory functions of Beat/Side proteins in ORN synapse formation.

Interestingly, analysis of previously reported antennal RNA-seq data (Deanhardt et al., 2023) from *Or47b* and *Or67d* mutants revealed differentially expressed *beat* and *side* genes (Figure S5F). We find that certain *beat* and *side* genes are up-regulated while others are down-regulated in olfactory receptor mutants (Figure S5F). These results suggest that these genes are responding to neural activity and might contribute to ORN-specific synapse development and maintenance. Notably, the transcriptional changes induced by OR-dependent neural activity, in addition to lineage factors, can contribute to the final combinatorial expression and synaptic function of Beat and Side proteins.

441

442 **Evolutionarily conserved expression of *beat/side* orthologs across insect ORNs**

443 Next, we sought to interrogate the ORN class-specific expression of *beats/sides* in other
444 species to gain some evolutionary insights into the regulation and function of these families of
445 IgSF proteins. Recently reported transcriptome atlas of ORNs in two additional insect species,
446 yellow fever mosquitoes *Aedes aegypti*, and clonal raider ants *Ooceraea biroi*, allowed us to
447 perform comparative analyses of *beat/side* expression in the peripheral olfactory tissue at
448 single-cell resolution. Yellow fever mosquito and clonal raider ants belong to the order Diptera
449 and a distant order Hymenoptera, and diverged from the fruit fly *Drosophila melanogaster*, a
450 Dipteran species, 260 million and 300 million years ago, respectively (Figure 5A). We first set
451 out to identify the bona fide orthologs of *beats/sides* in mosquitoes and ants. To do this, we
452 queried the protein sequence of *Drosophila* Beat-Ia and Side against the proteome database
453 of two other species and ran multiple sequence alignment after selecting the hits with
454 comparable lengths and similar AlphaFold-predicted structures (two Ig domains for Beats; five
455 Ig domains and one Fibronectin domain for Sides, also see Materials and Methods, Figure
456 S5A). We then built the phylogenetic tree of Beat/Side protein orthologs across the three
457 species. This analysis yielded 13 *beat* genes and 10 *side* genes in the yellow fever mosquito,
458 while the clonal raider ant has 10 *beats* and nine *sides* in its genome (Figure 5B, C). We
459 observed several notable gene duplication/loss events in these species. For example, there is
460 a single ant gene in the Beat-I clade, whereas there are three copies in mosquitoes and flies
461 (Figure 5B). In contrast, three ant genes encode the Side-IV clade and three mosquito genes
462 encode the Side-II clade, while only one fruit fly gene is in each clade (Figure 5C). Additionally,
463 the *side-V* gene appears to be lost in clonal raider ants (Figure 5C). The phylogenetic tree
464 indicates that: (1) gene duplication events generated ancestral *beat/side* paralogs earlier than
465 insect species divergence; (2) additional gene duplication/loss events also occurred post-
466 divergence of fruit fly, mosquito, and ant species.

467 Based on the phylogenetic tree, we renamed the mosquito and ant genes according to their
468 sequence similarities with the fruit fly orthologs (Table S1). We examined their expression in
469 ORNs using published single-cell datasets (Brahma et al., 2023; Herre et al., 2022). Strikingly,
470 we found combinatorial expression principles of *beat/side* genes in different ORN classes
471 across the three insect species are conserved (Figure 5D, E, and F; Figure S6B): (1) genes
472 that are not expressed in *Drosophila* ORNs, like *beat-Va/b/c*, *beat-VI*, and *side-VIII*, are also
473 not expressed in ORNs of yellow fever mosquitoes (*beat-Va/b*, *beat-VI*, *side-VIII*) or clonal
474 raider ants (*beat-V*, *beat-VIa/b*, *side-VIII*); (2) genes that are broadly expressed in *Drosophila*
475 ORNs, like *beat-VII*, *side-II*, and *side-III*, are also broadly expressed in ORNs of yellow fever
476 mosquitoes (*beat-VII*, *side-IIa/b*, and *side-III*) and clonal raider ants (*beat-VII*, *side-II*, and *side-*
477 *III*); (3) genes that are expressed in a restricted pattern across *Drosophila* ORNs, like *beat-*
478 *IIa/b*, beat-*IV*, and *side-IV* (Figure 2A, B), are also expressed in only a portion of ORN clusters
479 in mosquitoes (*beat-IIa*, beat-*IVa/b*, and *side-IV*) and ants (*beat-II*, beat-*IV*, and *side-IVb/c*).
480 Even though there is significant conservation of *beat/side* gene expression patterns across
481 ORNs, there are also a few exceptions. For example, *beat-Ia*, expressed in many ORN classes
482 in fruit flies and at high levels in restricted ORN classes in mosquitoes, is barely expressed in
483 ant ORNs. In addition, *side* is expressed in many *Drosophila* ORN classes but is undetectable
484 in mosquito and ant ORNs (Figure 5D, E, and F). These comparative analyses suggest that
485 both the evolutionarily conserved and plastic *beat* and *side* genes in peripheral sensory

neurons likely emerged due to genome evolution events that deleted or duplicated the members of the *beat* and *side* gene families and the regulatory sequences.

Interestingly, recent single-cell RNA-seq reports from clonal raider ant ORNs revealed regulatory differences in sensory receptor genes, where multiple *OR* transcripts are expressed in each ORN. In detail, ORNs that share a more similar transcriptome, and thus are clustered together in UMAP plots, usually express *ORs* located in a tandem array in the genome. In each ORN, a single start site is selected that transcribes *OR* genes downstream, while only the most upstream mRNA in the transcript is translated into a functional OR protein. This means the ORNs in each cluster are transcriptionally heterogeneous, containing multiple ORN classes defined by the functional expression of a singleton OR protein. To zoom in on ORN classes within each single-cell RNA-seq cluster, we plotted *beat/side* expression and the *ORs* of the tandem expressed in the cluster of each single cell as heatmaps (Figure 5G; Figure S6D). We found that each ORN class, defined by the expression of the most upstream *OR*, exhibits class-specific expression of *beat/sides*. For example, in cluster 3, the ORN class defined by the functional expression of Or5-9E109 doesn't express the ant *side-IVb,* whereas other ORN classes functionally expressing the adjacent Ors, Or5-9E108, Or5-9E107, and Or5-9E110 appear to be positive for this gene (Figure 5G top). Similarly, ORN classes defined by the functional expression of Or5-9E151 or Or5-9E150 in cluster 14 don't express the ant *beat-VII,* whereas many other ORN classes in this cluster do (Figure 5G bottom). This suggests, upon OR tandem choice, additional lineage mechanisms couple *OR* transcription initiation and *beat/side* expression specification in the clonal raider ant.

509 ## Discussion

510 In this study, we comprehensively delineated the expression pattern of *beat/side* family genes
511 in ORNs and PNs at single-cell and single-class levels. We found that each ORN or PN class
512 exhibits a unique combinatorial expression of *beats/sides*, and this *beat/side* profile appears to
513 be specified by the lineage-intrinsic genetic programs. In addition to analyzing the single-cell
514 transcriptome of ORNs and PNs, we also generated *MiMIC*-based gene trap driver lines to
515 probe the *beat/side* expression across ORNs and PNs *in vivo*. This approach enabled mapping
516 the *beat/side* expression to additional ORN/PN types not covered in the single-cell RNA-seq
517 datasets. Collectively, we found that *beat/side* profiles can diverge between some closely
518 related ORNs or some closely related PNs, suggesting that the Beat/Side combination may
519 add variability to cell surface codes, which biases their glomerular targeting. We also
520 investigated one interacting pair, Beat-IIa and Side-IV, based on their matching expression
521 pattern between partner ORNs and PNs, and found no apparent glomerular mistargeting in
522 knockdowns of *Beat-IIa* in ORNs or *Side-IV* in PNs. Yet, knockdown of the *side* gene in ORNs
523 resulted in diminished synapses in the antennal lobes, suggesting a role in synapse
524 development. Moreover, we found evolutionarily conserved expression patterns and ORN-
525 specific combinatorial signature principles for *beat* and *side* orthologs in the olfactory systems
526 of mosquitoes and ants, suggesting the shared genetic programs establishing the *beat/side*
527 profile. In sum, our studies implicate ORN/PN class-specific combinatorial Beat and Side
528 protein expression and their roles in olfactory circuit assembly.

529

530 **Developmental regulation of *beat/side* expression in ORNs and PNs**

531 We found the lineage-correlated expression profile of *beats/sides* in ORNs and PNs to be a
532 general principle, suggesting the lineage-specific programs in setting the *beat/side*
533 combinatorial expression. Our genetic labeling results and single-cell RNA-seq analyses also
534 reveal the existence of both shared and divergent expression patterns of *beat/side* between
535 closely related ORNs. We found that some sibling ORNs have different *beat/side* profiles and
536 project to distant antennal lobe regions, while some maintain the putative "template"
537 combinations found in many ORNs and project to neighboring or close glomeruli. Adjacently
538 born PNs can also have shared or divergent *beat/side* expression profiles. We therefore
539 propose that: (1) at the higher level of the developmental hierarchy, i.e., in ORN sensillar type
540 decisions or PN lineage specification decisions, the *beat/*side "template" is set by lineage-
541 specific factors; (2) the latest common precursor of ORNs (i.e. sensilla subtype precursors) or
542 PNs may have diverse intrinsic factors that bias the expression of additional *beat/side*
543 combinatorial expression while some do not; (3) such that at the final terminal selection
544 decision, Beat/Side combinations may mediate the synapse programs in closely related ORNs
545 or PNs. Furthermore, expression of additional cell surface proteins can increase the cell
546 surface protein repertoire, further diversifying neuronal identification tags displayed on neurons
547 utilized during circuit assembly. This two-step model, setting the lineage-specific cell surface
548 molecular template, followed by within-lineage diversification, seems to be an efficient way to
549 establish the cell type-specific surface molecular repertoire by genetically deterministic
550 programs. This might be a developmental strategy to coordinate the combinatorial expression
551 of duplicated paralogs.

552

553 **Molecular complexity and redundancy of Beats/Sides as cell surface "codes"**

554 Side was first identified as the postsynaptic ligand, expressed in muscles, to attract motor
555 neurons. Motor neurons expressing the receptor Beat-Ia follow the Side-labeled muscles and
556 leave axonal fasciculations to innervate muscle targets (de Jong et al., 2005; Fambrough and
557 Goodman, 1996; Pipes et al., 2001; Siebert et al., 2009; Sink et al., 2001). The embryonic
558 expression pattern analysis expanding to other Beat/Side family paralogs also suggests that
559 Beats are neuronal receptors for Sides expressed on peripheral tissues (Li et al., 2017b). For
560 example, Side-VI is expressed in muscle fibers while its receptors, Beat-Vs, are expressed in
561 motor neurons (Li et al., 2017b). This evidence jointly points to the fact that Sides are present
562 primarily in postsynaptic sites, signaling to presynaptic Beats to promote synaptogenesis.
563 Outside of the neuromuscular junction, recent reports in the fly visual circuits also suggest
564 presynaptic Side-II and postsynaptic Beat-VI mediate synaptic recognition (Yoo et al., 2023).
565 Additional studies revealed presynaptic (photoreceptor-expressed) Side-IV can induce
566 synaptogenesis by acting as both ligands and receptors when interacting with postsynaptic
567 Beat-IIa/b, forming synaptogenic complexes through their interactions with Beat-IIa/b and
568 coreceptor Kirre (Osaka et al., 2024).

569 In the olfactory circuits consisting of ORNs and PNs, we found that *beat* and *side* genes are
570 expressed in the same neurons. ORNs generally lack Beats but are abundant for Sides. This
571 would point to a model where Sides primarily interact with PN-expressed Beats. However,
572 ORNs do express a few Beats with their binding partner Sides as well as some orphan Beats.
573 And PNs generally express both Sides and Beats. Similarly, DIPs and Dprs can also be
574 expressed in the same cells, like adult ORNs (Barish et al., 2018) and larval motor/sensory
575 neurons (Wang et al., 2022). There are several possible functional explanations based on Beat
576 and Side interactions. First, Sides and Beats may have different subcellular localizations that
577 position places of protein-protein interactions and cellular functions. For example, Beats might
578 localize to PN dendrites to interact with Sides on ORN axon terminals, while Side proteins
579 localized to PN axon terminals may interact with Beats expressed on the dendrites of third-
580 order neurons. If this is the case, this binary subcellular preference may vary in different cell
581 types to mediate interactions with other neurons. In motor neurons, Beats are preferentially
582 sorted to axon terminals, whereas in the central nervous system or sensory neurons, Sides are
583 preferentially sorted to axon terminals. Second, Beats/Sides can function in both dendrites and
584 axons simultaneously and act as ligands and receptors bidirectionally. This points to a model in
585 which the combinatorial code of multiple surface proteins establishes synaptic specificity
586 recognition, likely by providing differential adhesive forces. Third, Beats and Sides in the same
587 neuron might interact *in cis* on the same membrane in addition to their interactions *in trans* with
588 Beat/Side proteins on other neurons. Interestingly, a recent study showed that DIP-Dpr
589 interactions favor *cis* over *trans* when present in the same cell (Morano et al., 2025). It might
590 also be the case that when Beats/Sides are localized together in the same membrane regions,
591 it is the competition between *cis* and *trans* interactions with all present binding partners in the
592 proximity that sets the "net" Beat/Side surface codes.

593 Additionally, combinations of cell surface adhesion molecules can form multi-molecular
594 complexes, so the absence of any component may not abolish but just reduce the recognition
595 efficacy or shift these complexes to new stoichiometric configurations (Honig and Shapiro,
596 2020; Sanes and Zipursky, 2020). Given this sophisticated context, it is not surprising that
597 removing a single gene is insufficient to change glomerular organization. Regarding Beat/Side

combinatorial complexity, deleting *side-IV* in PNs or *beat-IIa* in ORNs doesn't ambiguate DM1 from adjacent glomeruli (Figure 4), and ORN-PN synaptic matching can still occur. Thus, the promiscuous and redundant functions of the Beat/Side family have the capacity to form an error-tolerant adhesion code, enabling recognition robustness. These are supported by our efforts to perturb a single *beat/side* gene that caused subtle to no defects (Figure S4A). Previously reported screens for CSMs mediating ORN-PN synaptic matching also didn't report any defects in glomerular targeting with any *beat/side* knockdowns (Xie et al., 2019). A recent study has shown that collective manipulation of multiple cell surface molecules substantially rewires an ORN-PN circuit, while loss-of-function of a single one only causes minor mistargeting (Li et al., 2025; Lyu et al., 2025). Our expression dataset provides a roadmap to further crack the combinatorial coding nature of Beats and Sides by multiplexing perturbation.

Intriguingly, we observed weakened synapses in the antennal lobes when we knocked down the *side* gene, which suggests that Side and Beat protein interactions might mediate synapse formation in the olfactory circuits. This is supported by other recent studies in the visual system reporting Side-IV as a synapse-inducing protein (Osaka et al., 2024), and that Beat-VI expression gradients regulate synaptic density gradients through their interactions with Side-II (Dombrovski et al., 2025). These results suggest that Beat/Side interactions may inherently have synaptogenic functions and participate in the subglomerular synaptic organization during olfactory circuit development. Furthermore, since many *beats/sides* show persistent high expression levels from the pupal stage to adulthood, they might be recruited for synapse induction, formation, and stabilization, and modulated by OR signaling and/or neuronal activity.

Evolutionarily conserved expression of *beats/sides* in ORNs of insects

We observed similar combinatorial expression patterns across ORN clusters among recently duplicated paralogs within the same species, as well as orthologs in ants and mosquitoes, suggesting evolutionarily conserved mechanisms that regulate their expression in ORNs. We speculate that ancestral paralogs of *beats/sides* with their regulatory elements acquired cell-type-specific expression patterns, which were generally retained during evolution and shared between species. More recent gene duplication events after speciation generated additional paralogs within each *beat/side* clade, where we observe both shared (*Drosophila beat-IIIa/b/c* and *beat-Va/b/c*, *A. aegypti beat-IVa/b* and *side-IIa/b*, *O. biroi beat-VIa/b*) and divergent expression patterns (*A. aegypti beat-Ia1/a2* and *side-IIb/c*, O*. biroi side-IVa/b/c*). Though some *beat* and *side* genes exhibit evolutionary plasticity in their expression patterns, conservation of the expression of many *beat/side* genes in ORNs appears to be a general rule. This implies that there are selection pressures on the operative roles that these genes play in the ORN development and function.

Interestingly, in clonal raider ants, there appear to be two steps specifying the ORN fate: first, choosing the OR tandem and second, choosing the OR transcription start site within the tandem. Our results suggest that the *beat/side* ortholog expression is also coupled with these two steps. *Drosophila* appears to exploit the genetically deterministic strategy to specify the combinatorial expression of cell surface proteins to organize diverse ORN classes into the hardwired circuits. However, when neuronal types become more heterogeneous, possibly exceeding a diversity limit, such a solely genetics-dependent program may be incapable. This is likely to be the case in the olfactory systems of ants with many more classes of ORNs.

Recent studies suggest ORs themselves may play instructional roles in glomerular targeting in ants, different from fruit flies but similar to mammals (Duan and Volkan, 2020; Ryba et al., 2020; Trible et al., 2017; Yan et al., 2017). It is possible that the ORN class-specific expression of *beat/side* is also regulated by ORs in ants.

Limitations of the study

Many *beat/side* genes transcribe multiple splice isoforms, which adds an additional layer of molecular diversity. This study didn't examine the expression of *beat* and *side* splice isoforms in the olfactory system. Our transgenic *GAL4* driver lines generally trap the common regions across isoforms and cannot address isoform-specific expression. Single-cell RNA-seq approaches that resolve *beat* and *side* splice isoforms or expression analysis of isoform-specific *GAL4*s would be needed to this end.

This study only reveals the *beat* and *side* expression at the transcriptional level and does not address the Beat and Side protein-level distributions. Some studies reported large discrepancies between transcripts encoding surface molecules and their protein abundance in developing PNs (Li et al., 2020b), suggesting regulation at the level of translation, protein stability, modification, sorting, and delivery to the cell surface.

Future directions

In the future, it will be interesting to investigate how regulatory sequence evolution contributes to the conserved and divergent expression patterns of *beat* and *side* paralogs across species. Additional biochemical characterization of Beats/Sides protein-protein interactions in different insect species will provide novel insights into the co-evolution of coding sequences with regulatory sequences to reconcile their functional evolution in circuit assembly.

Understanding the biochemical features of Beat and Side proteins will greatly inform the functional analysis in the circuit assembly context. This includes developing a more sensitive and specific test to deorphanize Beat-Side interactions, characterizing whether Beats/Sides are transmembrane proteins or membrane-anchored like DIPs/Dprs (Lobb-Rabe et al., 2024), and testing whether they interact *in trans* and/or *in cis*. If they are transmembrane proteins, then how are their functions mediated by intracellular and extracellular protein domains? Proximity labeling-based proteome profiling, like BIO-ID, can identify these protein interactors, which will inform further functional investigation. A recent study reported that the N-terminal domain of Beat-Ia is localized to the cell surface while the C-terminus accumulates in the nucleus; this implies that Beat-Ia might undergo proteolytic cleavage for proper function (Heymann et al., 2022). Future biochemical, genetic, and neurophysiological studies will help reveal the function of Beat and Side proteins in recognition specificity and synaptic transmission.

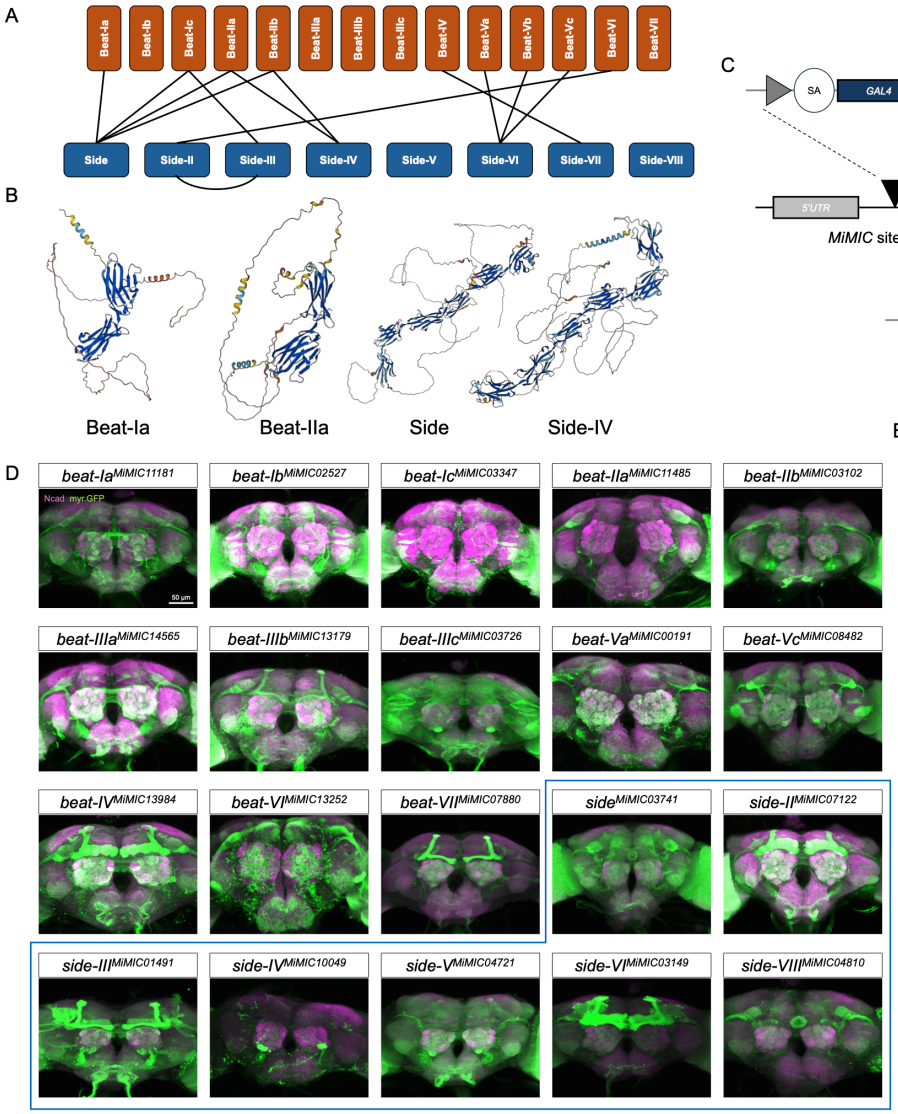

E

MiMIC-GAL4	insertion site	affected isoforms /total isoforms
beat-Ia^{MiMIC11181}	coding intron	2/2
beat-Ib^{MiMIC02527}	coding intron	2/2
beat-Ic^{MiMIC03347}	5' UTR	3/3
beat-IIa^{MiMIC11485}	coding intron	2/2
beat-IIb^{MiMIC03102}	coding intron	1/2
beat-IIIa^{MiMIC14565}	coding intron	2/2
beat-IIIb^{MiMIC13179}	coding intron	2/2
beat-IIIc^{MiMIC03726}	coding intron	2/2
beat-IV^{MiMIC13984}	coding intron	2/2
beat-Va^{MiMIC00191}	coding intron	3/3
beat-Vc^{MiMIC08482}	coding intron	1/1
beat-VI^{MiMIC13252}	5' UTR	2/2
beat-VII^{MiMIC07880}	coding intron	1/1
side^{MiMIC03741}	coding intron	4/4
side-II^{MiMIC07122}	coding intron	3/3
side-III^{MiMIC01491}	5' UTR	1/1
side-IV^{MiMIC10049}	5' UTR	2/2
side-V^{MiMIC04721}	coding intron	2/2
side-VI^{MiMIC03149}	coding intron	2/2
side-VIII^{MiMIC04810}	coding intron	4/4

Figure 1. Beats/Sides are heterophilically interacting IgSF proteins.
(A) Schematics showing the known interactions between Beat and Side proteins.
(B) AlphaFold-predicted structures of example Beat and Side proteins. Beats have two extracellular Ig domains, while Sides' extracellular parts consist of five Ig domains and one Fibronectin type III domain. Transmembrane and intracellular domains are poorly predicted. Structures were downloaded from AlphaFold.ebi.ac.uk (Jumper et al., 2021).
(C) Schematic showing *MiMIC*-based insertion of the GAL4-coding construct into either the 5' UTR or the "coding" intron, which will hijack the expression of the host gene. If *GAL4* is inserted into introns within the 5' UTR, the *GAL4* artificial exon will first be kept from splicing and then will be translated as it has its own start codon. If the in-frame *T2A-GAL4* construct is inserted into an intron between two coding exons, this whole artificial exon will also be prevented from splicing and then translated along with the upstream coding sequence. During translation, the *T2A* sequence causes the ribosome to fail at synthesizing the peptide bond, and thereby, a truncated peptide of the host gene and a GAL4 protein will be produced separately. In both cases, GAL4 is expected to be expressed in the same cell where the native

696 gene is expressed. SA, splice acceptor; SD, splice donor; pA, Hsp70 polyadenylation signal to
697 terminate transcription; linker sequence ensures *T2A-GAL4* will be translated in frame.
698 **(D)** Expression pattern of each *beat/side* in the brain revealed by *beat/side-MiMIC-GAL4*.
699 Green is the GFP signal driven by the gene trap GAL4, and magenta is anti-Ncad staining
700 showing the brain architecture.
701 **(E)** Table summary of the insertion site and the isoforms labeled by each *beat/side-MiMIC-*
702 *GAL4.*
703

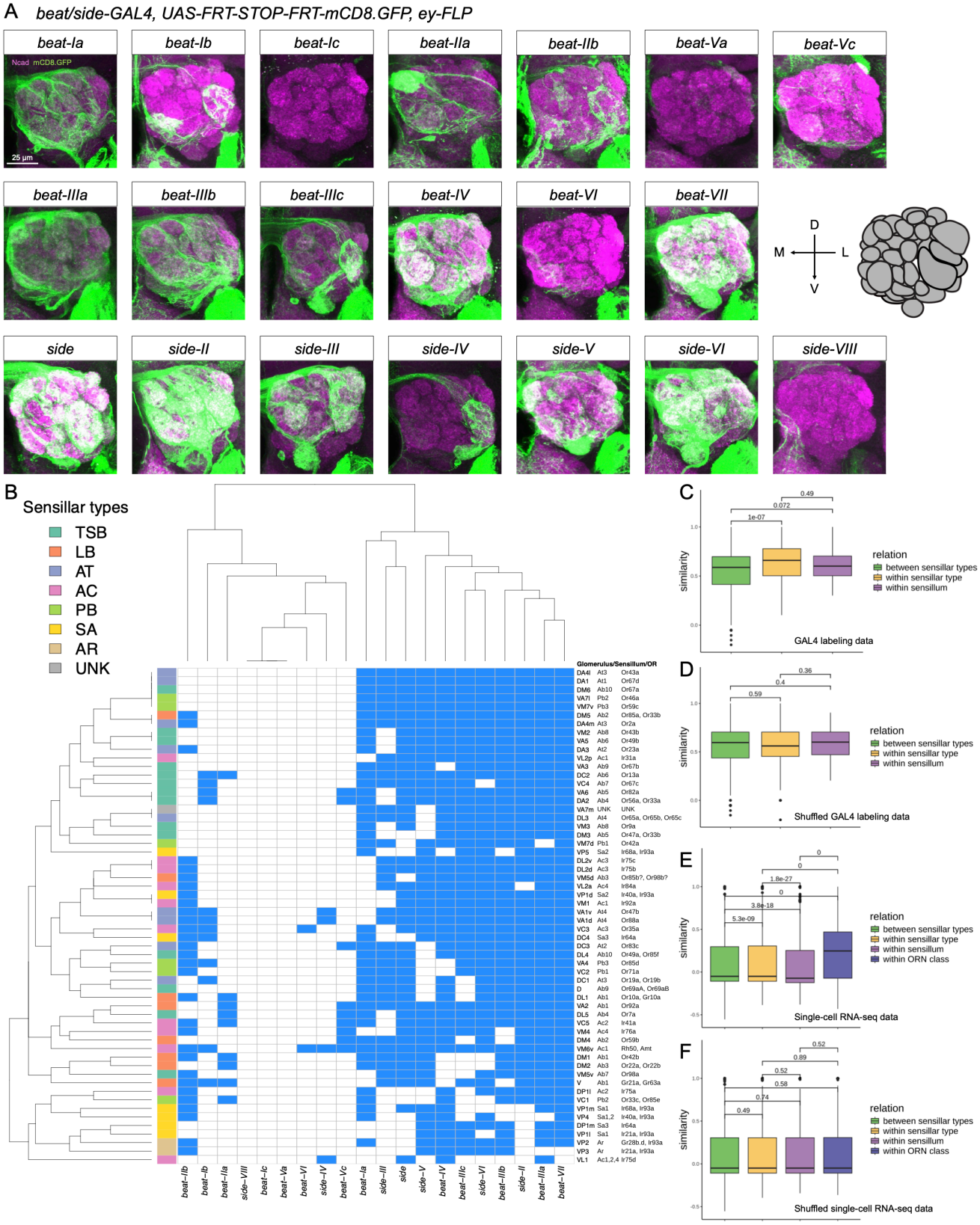
A
beat/side-GAL4, UAS-FRT-STOP-FRT-mCD8.GFP, ey-FLP
beat-Ia
beat-Ib
beat-Ic
beat-IIa
beat-IIb
beat-Va
beat-Vc
Ncad mCD8.GFP
25 µm
beat-IIIa
beat-IIIb
beat-IIIc
beat-IV
beat-VI
beat-VII
D
M
L
V
side
side-II
side-III
side-IV
side-V
side-VI
side-VIII
B
Sensillar types
TSB
LB
AT
AC
PB
SA
AR
UNK
Glomerulus/Sensillum/OR
C
similarity
relation
between sensillar types
within sensillar type
within sensillum
GAL4 labeling data
D
Shuffled GAL4 labeling data
E
within ORN class
Single-cell RNA-seq data
F
Shuffled single-cell RNA-seq data

704

Figure 2. Lineage-dependent combinatorial expression of *beats/sides* across ORN classes.

(A) A glomerular map of *beat/side* expression in ORNs revealed by transgenic *GAL4* driver lines. Glomerular structures are stained by anti-Ncad (magenta). Anti-GFP staining (green) highlights the glomeruli innervated by the indicated *beat/side*-positive ORNs. All antennal lobes shown are right antennal lobes. M, medial; L, lateral; D, dorsal; V, ventral. Each image is shown as the intensity projection over the Z-axis.

(B) Hierarchical clustering of *beat/side* expression across ORNs based on the GAL4 labeling analysis. Row and column dendrograms are based on hierarchical clustering results. ORN class (named by its target glomerulus), the sensillum (sensillar subtype) where the ORN is housed, and the corresponding ORs expressed are shown on the right. The left row label is color-coded based on the ORN lineage. Blue means positive for the given gene expression, whereas white denotes negative. TSB, thin and small basiconics; LB, large basiconics; AT, antennal trichoids; AC, antennal coeloconics; PB, palp basiconics; SA, sacculus; AR, arista; UNK, unknown. VM6 glomerulus has been recently shown to be comprised of three subglomeruli, VM6v, VM6m, and VM6l, innervated by ORNs from Ac1 sensillum and Sacculus chamber III, respectively (Task et al., 2022). As it is difficult to distinguish Ac1-originated VM6v from the other two without additional colabeling, we counted VM6 as a single intact glomerulus for simplicity.

(C) Similarity (Pearson's correlation) of *beat/side* expression between ORN class pairs based on the expression matrix of (B) in three relation categories.

(D) Similarity (Pearson's correlation) of *beat/side* expression between ORN class pairs based on the expression matrix of (B), with row labels shuffled in three relation categories.

(E) Similarity (Spearman's correlation) of *beat/side* expression between ORN cell pairs based on the single-cell RNA-seq in four relation categories.

(F) Similarity (Spearman's correlation) of *beat/side* expression between ORN cell pairs based on the single-cell RNA-seq with ORN class annotation shuffled in four relation categories. In (C) to (F), P values from the Mann-Whitney U test of each comparison are shown.

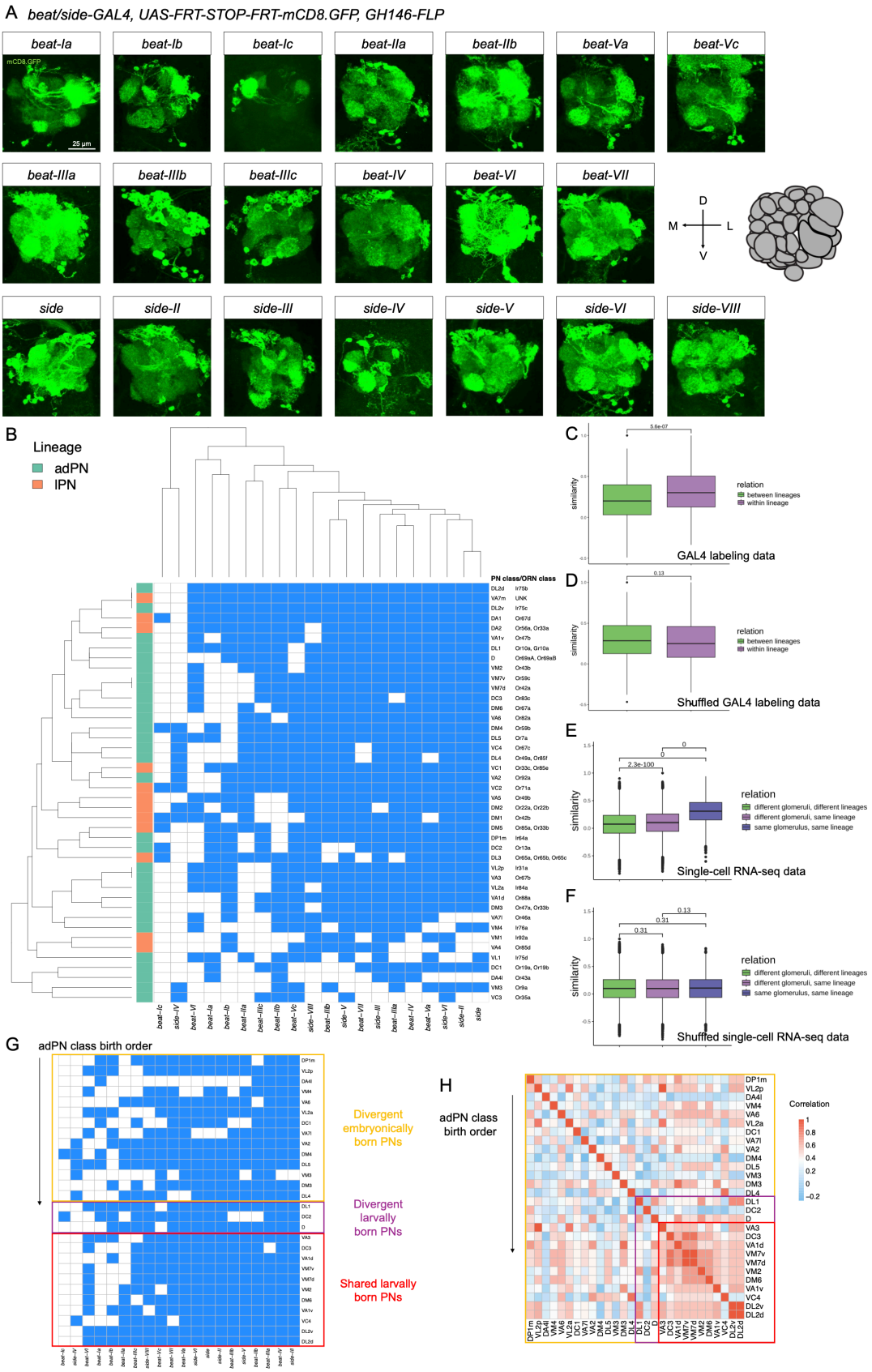
A beat/side-GAL4, UAS-FRT-STOP-FRT-mCD8.GFP, GH146-FLP
beat-Ia
beat-Ib
beat-Ic
beat-IIa
beat-IIb
beat-Va
beat-Vc
beat-IIIa
beat-IIIb
beat-IIIc
beat-IV
beat-VI
beat-VII
side
side-II
side-III
side-IV
side-V
side-VI
side-VIII
mCD8.GFP
25 µm
D
M
L
V
B
Lineage
adPN
lPN
PN class/ORN class
C
similarity
relation
between lineages
within lineage
GAL4 labeling data
D
Shuffled GAL4 labeling data
E
different glomeruli, different lineages
different glomeruli, same lineage
same glomerulus, same lineage
Single-cell RNA-seq data
F
Shuffled single-cell RNA-seq data
G
adPN class birth order
Divergent embryonically born PNs
Divergent larvally born PNs
Shared larvally born PNs
H
Correlation

735 **Figure 3. Lineage-correlated combinatorial expression of *beats/sides* across PN**
736 **classes.**
737 **(A)** A glomerular map of *beat/side* expression in PNs revealed by transgenic *GAL4* driver lines.
738 Only the GFP signal (green) highlights the glomeruli innervated by the indicated *beat/side*-
739 positive PNs. Neuropils were stained with anti-Ncad antibody to help determine the glomerular
740 identity but are not shown for visualization contrast. All antennal lobes shown are right
741 antennal lobes. M, medial; L, lateral; D, dorsal; V, ventral. Each image is shown as the intensity
742 projection over the Z-axis.
743 **(B)** Hierarchical clustering of *beat/side* expression across PNs based on the GAL4 labeling
744 analysis. Row and column dendrograms are based on hierarchical clustering results. PN class
745 and its matching ORN class (named by corresponding ORs expressed) are shown on the right.
746 The left row label is color-coded based on the uniglomerular PN lineage. Blue means positive
747 for the given gene expression, whereas white denotes negative.
748 **(C)** Similarity (Pearson's correlation) of *beat/side* expression between PN class pairs based on
749 the expression matrix of (B) in two relation categories.
750 **(D)** Similarity (Pearson's correlation) of *beat/side* expression between PN class pairs based on
751 the expression matrix of (B) with row labels shuffled in two relation categories.
752 **(E)** Similarity (Spearman's correlation) of *beat/side* expression between PN cell pairs based on
753 the single-cell RNA-seq in three relation categories.
754 **(F)** Similarity (Spearman's correlation) of *beat/side* expression between PN cell pairs based on
755 the single-cell RNA-seq with ORN class annotation shuffled in three relation categories. In (C)
756 to (F), P values from the Mann-Whitney U test of each comparison are shown.
757 **(G)** The summary matrix is replotted from (B), but only PN classes from the adPN lineage with
758 decoded birth order are shown. Rows representing PN classes are ordered based on the
759 known birth sequence, while *beat/side* genes are hierarchically clustered.
760 **(H)** Heatmap showing the Pearson's correlation matrix between PN classes based on the
761 *beat/side* expression. PN classes are the same as (G) and are ordered based on the birth
762 sequence.
763

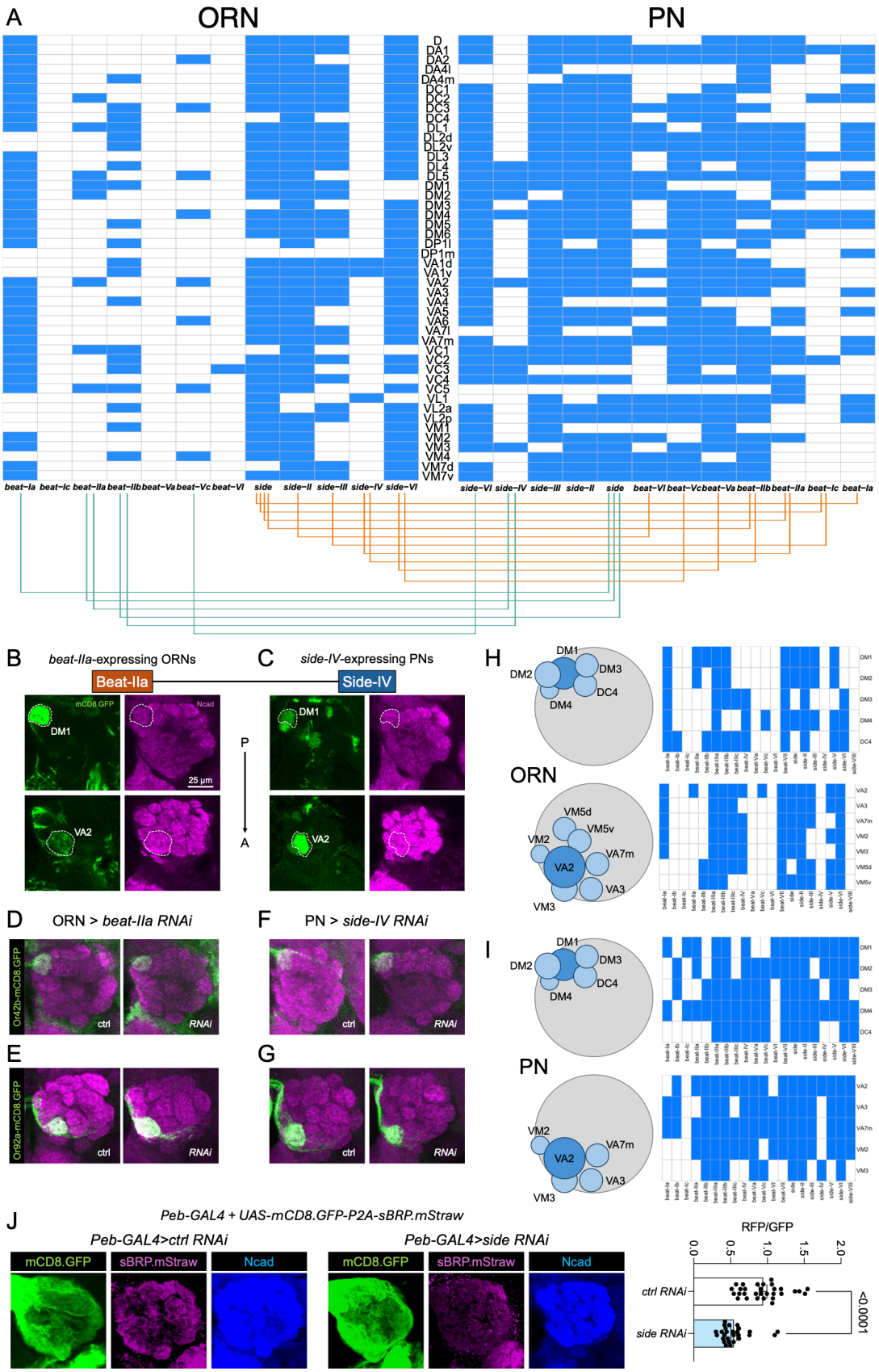
A
ORN
PN
D
DA1
DA2
DA4l
DA4m
DC1
DC2
DC3
DC4
DL1
DL2d
DL2v
DL3
DL4
DL5
DM1
DM2
DM3
DM4
DM5
DM6
DP1l
DP1m
VA1d
VA1v
VA2
VA3
VA4
VA5
VA6
VA7l
VA7m
VC1
VC2
VC3
VC4
VC5
VL1
VL2a
VL2p
VM1
VM2
VM3
VM4
VM7d
VM7v
beat−Ia beat−Ic beat−IIa beat−IIb beat−Va beat−Vc beat−VI side side−II side−III side−IV side−VI
side−VI side−IV side−III side−II side beat−VI beat−Vc beat−Va beat−IIb beat−IIa beat−Ic beat−Ia
B
beat-IIa-expressing ORNs
Beat-IIa
C
side-IV-expressing PNs
Side-IV
mCD8.GFP
Ncad
DM1
VA2
25 µm
P
A
H
DM1
DM2
DM3
DC4
DM4
ORN
VM5d
VM5v
VM2
VA7m
VA2
VA3
VM3
I
PN
D
ORN > beat-IIa RNAi
F
PN > side-IV RNAi
Or42b-mCD8.GFP
ctrl
RNAi
E
G
Or92a-mCD8.GFP
J
Peb-GAL4 + UAS-mCD8.GFP-P2A-sBRP.mStraw
Peb-GAL4>ctrl RNAi
Peb-GAL4>side RNAi
mCD8.GFP
sBRP.mStraw
Ncad
RFP/GFP
0.0
0.5
1.0
1.5
2.0
ctrl RNAi
side RNAi
<0.0001

764

765 **Figure 4. Beats-Sides interactions between matching ORN-PN partners can form a**
766 **redundant, error-tolerant surface "barcode", enabling recognition robustness and**
767 **mediating synaptogenesis.**
768 **(A)** Potential trans-synaptic Beat/Side interactions between matching ORN-PN classes
769 targeting each glomerulus. The ORN (left) and PN (right) profile of beat/side expression is
770 based on Figures 2B and 3B, but it is replotted to highlight the ORN class and PN class
771 innervating the same glomerulus. Based on *in vitro* biochemical characterization (Figure 1A),
772 known binding interactions between Beats and Sides are indicated as lines. Green lines
773 represent Beats -> Sides interactions, and red lines represent Sides -> Beats interactions
774 (ORN -> PN).
775 **(B)** ORNs targeting DM1 and VA2 glomeruli expressing *beat-IIa*, labeled by the intersection of
776 *beat-IIa-T2A-GAL4* and *ey-FLP* to drive *UAS>STOP>mCD8.GFP*. Scale bar representing 25
777 µm also applies to each antennal lobe panel in (C) to (G) and (J).
778 **(C)** PNs targeting DM1 and VA2 glomeruli expressing *side-IV*, labeled by the intersection of
779 *side-IV-GAL4* and *GH146-FLP* to drive *UAS>STOP>mCD8.GFP*. In (B) and (C), the left
780 columns show anti-GFP staining (green) and the right columns show anti-Ncad staining
781 (magenta).
782 **(D, E)** Knockdown of *beat-IIa* in ORNs by a pan-ORN driver, *peb-GAL4,* while labeling Or42b
783 ORNs targeting DM1 glomerulus (D) and Or92a ORNs targeting VA2 glomerulus (E).
784 **(F, G)** Knockdown of *side-IV* in PNs by a PN driver *GH146-GAL4* while labeling Or42b ORNs
785 targeting DM1 glomerulus (F) and Or92a ORNs targeting VA2 glomerulus (G). Neuropils were
786 stained with anti-Ncad antibody, shown in magenta. Representative images from 7 to 12 brains
787 examined in each condition are shown (D-G).
788 **(H)** The Beat/Side "barcode" in ORNs targeting DM1 or VA2 and their neighboring glomeruli,
789 based on the *beat/side-GAL4* labeling results in Figure 2B.
790 **(I)** The Beat/Side "barcode" in PNs targeting DM1 or VA2 and their neighboring glomeruli
791 based on the *beat/side-GAL4* labeling results in Figure 3B. VM5d/v PN expression is unknown
792 because these glomeruli are not labeled by the PN-FLP we used. In (H) and (I), the
793 schematics show the antennal lobe (gray circle) and the relative positions of the indicated
794 glomeruli (blue circles).
795 **(J)** Representative antennal lobes and quantification showing the effects of knockdown of *side*
796 on gross glomerular synaptic density, visualized by the membrane marker GFP and
797 presynaptic marker RFP. Each dot is a single antennal lobe. N = 30 and 27 antennal lobes,
798 respectively. P-value from the unpaired t-test between groups is shown.
799

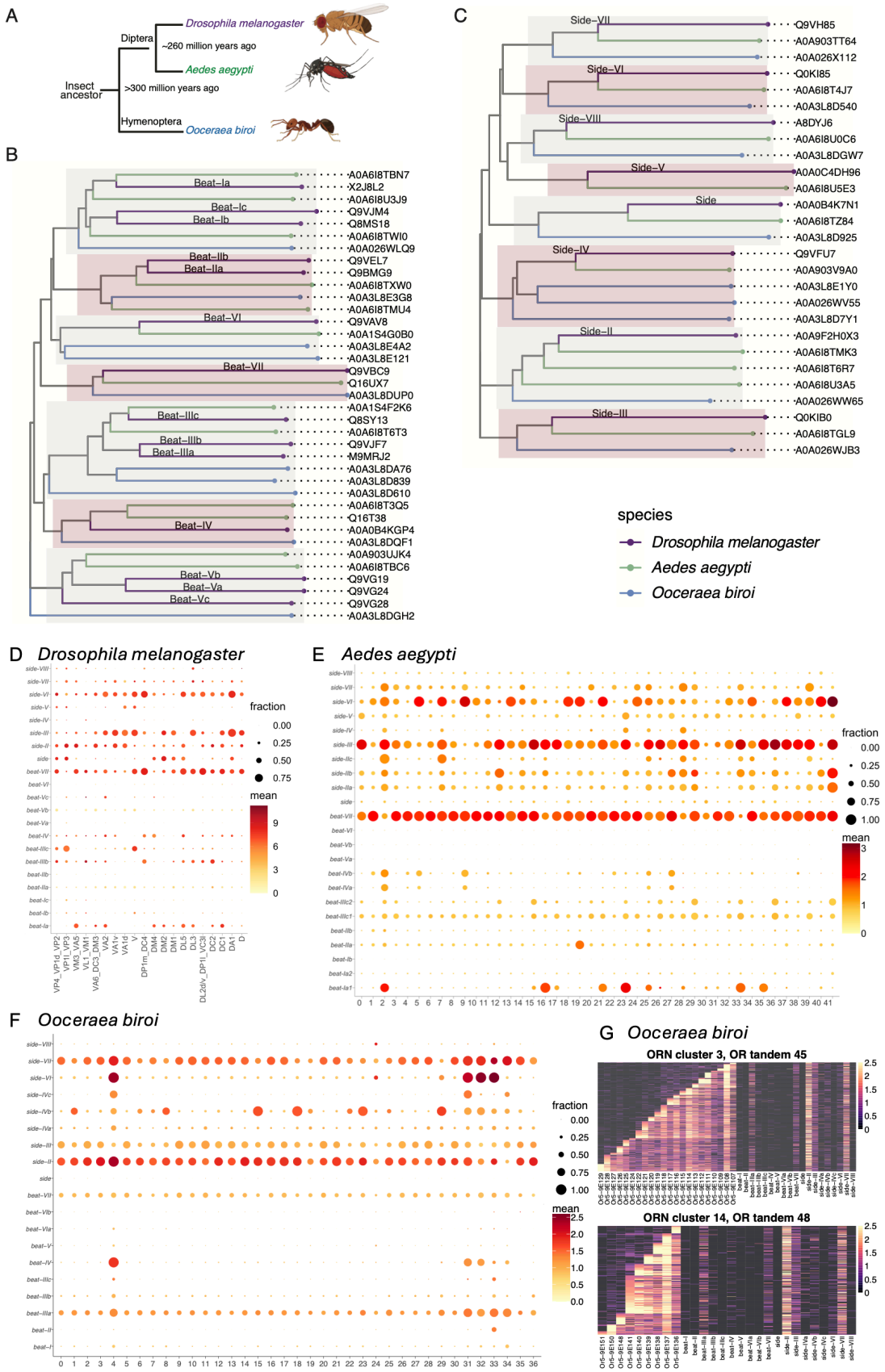
A
Drosophila melanogaster
Diptera
~260 million years ago
Aedes aegypti
Insect ancestor
>300 million years ago
Hymenoptera
Ooceraea biroi
B
Beat–Ia
Beat–Ic
Beat–Ib
Beat–IIb
Beat–IIa
Beat–VI
Beat–VII
Beat–IIIc
Beat–IIIb
Beat–IIIa
Beat–IV
Beat–Vb
Beat–Va
Beat–Vc
A0A6I8TBN7
X2J8L2
A0A6I8U3J9
Q9VJM4
Q8MS18
A0A6I8TWI0
A0A026WLQ9
Q9VEL7
Q9BMG9
A0A6I8TXW0
A0A3L8E3G8
A0A6I8TMU4
Q9VAV8
A0A1S4G0B0
A0A3L8E4A2
A0A3L8E121
Q9VBC9
Q16UX7
A0A3L8DUP0
A0A1S4F2K6
Q8SY13
A0A6I8T6T3
Q9VJF7
M9MRJ2
A0A3L8DA76
A0A3L8D839
A0A3L8D610
A0A6I8T3Q5
Q16T38
A0A0B4KGP4
A0A3L8DQF1
A0A903UJK4
A0A6I8TBC6
Q9VG19
Q9VG24
Q9VG28
A0A3L8DGH2
C
Side–VII
Side–VI
Side–VIII
Side–V
Side
Side–IV
Side–II
Side–III
Q9VH85
A0A903TT64
A0A026X112
Q0KI85
A0A6I8T4J7
A0A3L8D540
A8DYJ6
A0A6I8U0C6
A0A3L8DGW7
A0A0C4DH96
A0A6I8U5E3
A0A0B4K7N1
A0A6I8TZ84
A0A3L8D925
Q9VFU7
A0A903V9A0
A0A3L8E1Y0
A0A026WV55
A0A3L8D7Y1
A0A9F2H0X3
A0A6I8TMK3
A0A6I8T6R7
A0A6I8U3A5
A0A026WW65
Q0KIB0
A0A6I8TGL9
A0A026WJB3
species
Drosophila melanogaster
Aedes aegypti
Ooceraea biroi
D Drosophila melanogaster
fraction
mean
E Aedes aegypti
fraction
mean
F Ooceraea biroi
fraction
mean
G Ooceraea biroi
ORN cluster 3, OR tandem 45
ORN cluster 14, OR tandem 48

800

Figure 5. Evolutionarily conserved expression pattern of *beats/sides* across ORNs in insects.

(A) Schematic phylogeny showing the evolutionary distance among three insect species.

(B) Phylogeny tree of Beat orthologs in fruit flies *Drosophila melanogaster*, yellow fever mosquitoes *Aedes aegypti*, and clonal raider ants *Ooceraea biroi*. Each leaf is color-coded by the species, shown in the bottom right legend. Each ortholog is displayed as the UniProt protein ID, while the known *Drosophila* Beat names are labeled on the corresponding branch.

(C) Phylogenetic tree of Side orthologs across three insect species.

(D) Expression of *beats/sides* in the adult ORN classes of fruit flies based on the single-cell RNA-seq data from (McLaughlin et al., 2021). Each row is a gene, and each column represents an annotated ORN class. The size of each dot represents the percentage of positive cells in the given class (log2(CPM+1) > 0.5), and the color denotes the mean expression levels. This panel was reproduced from Figure S2B for comparison.

(E) Expression of *beats/sides* in the adult ORN clusters of yellow mosquitoes based on the single-cell RNA-seq data from (Herre et al., 2022). The mosquito *beats/sides* were renamed based on their phylogenetic relations with the fruit fly orthologs.

(F) Expression of *beats/sides* in the adult ORN clusters of clonal raider ants based on the single-cell RNA-seq data from (Brahma et al., 2023). The ant *beats/sides* were renamed based on their phylogenetic relations with the fruit fly orthologs.

(G) Heatmap showing the expression of *beats/sides* and *OR* genes in two example ORN clusters of clonal raider ants, based on the single-cell RNA-seq data from (Brahma et al., 2023). *OR* genes are ordered from 5’ end to 3’ end in the tandem.

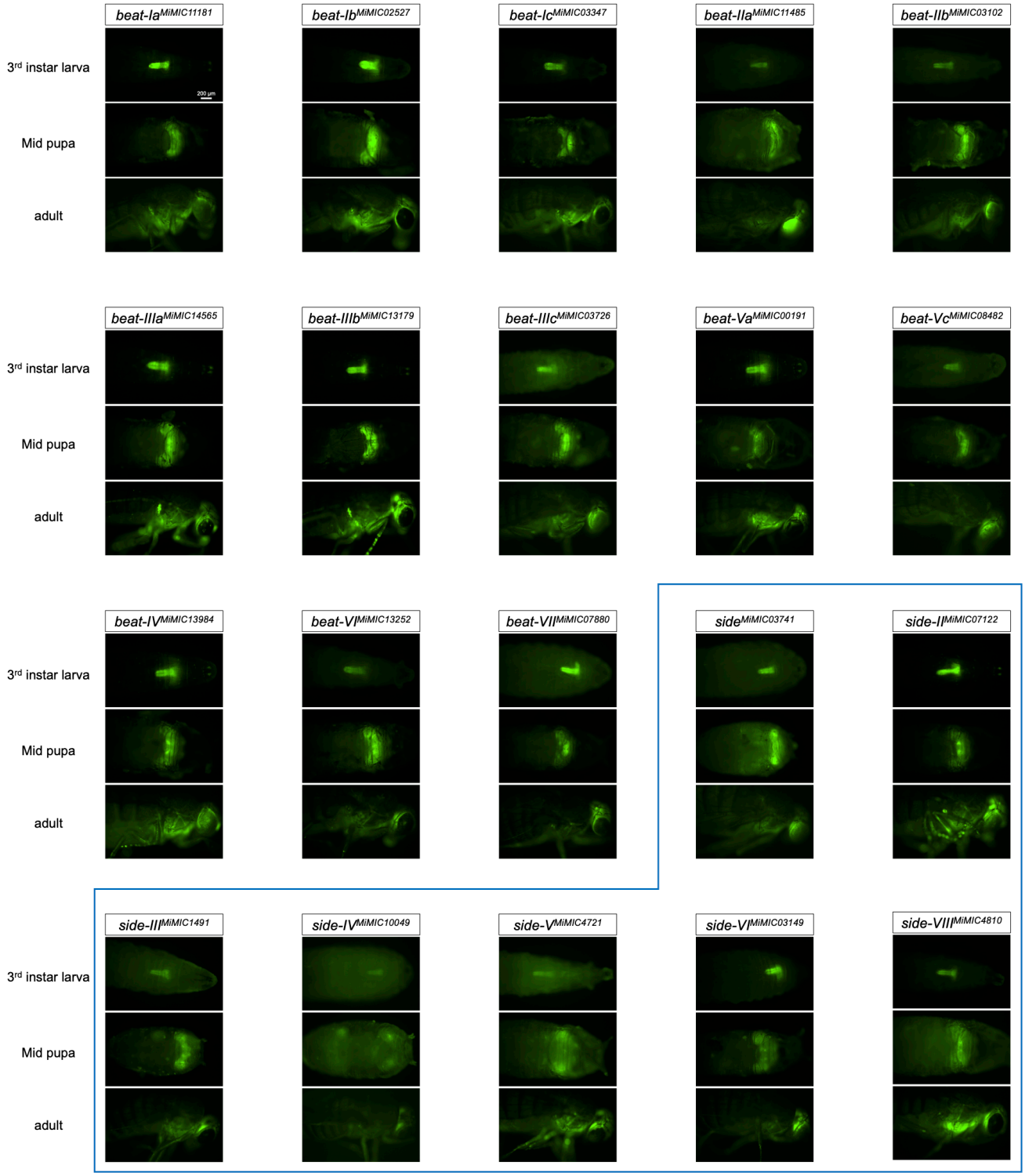

Figure S1. *beat* and *side* expression are enriched in the nervous system throughout development revealed by *MiMIC*-based gene trap drivers. Related to Figure 1.
Whole-animal fluorescence images of each *beat/side* gene trap GAL4 driving myr.GFP in the 3rd instar larval stage, mid-pupal stage (~48h APF), and adult.

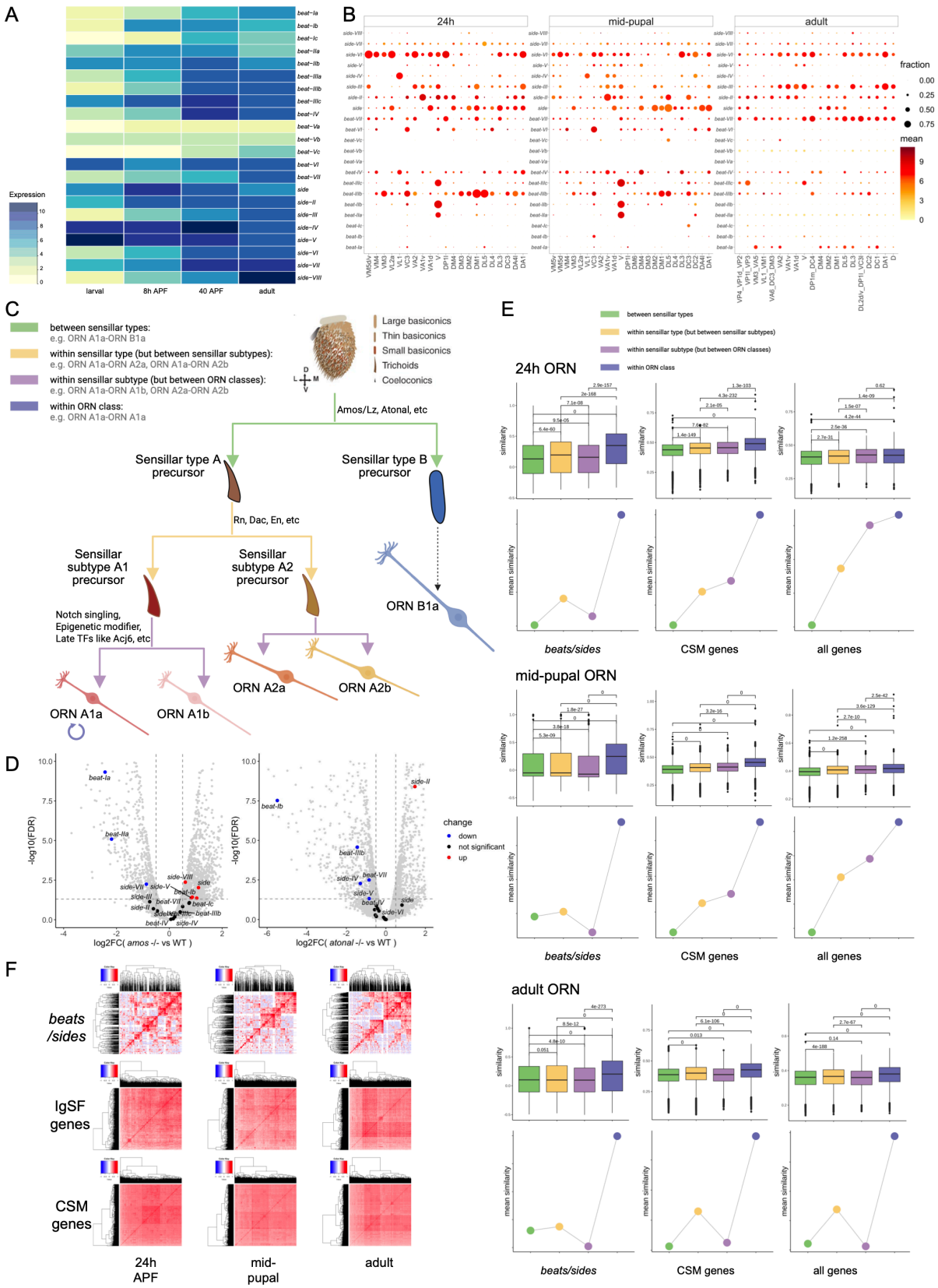
A
Expression
larval
8h APF
40 APF
adult
B
24h
mid-pupal
adult
fraction
mean
C
between sensillar types:
e.g. ORN A1a-ORN B1a
within sensillar type (but between sensillar subtypes):
e.g. ORN A1a-ORN A2a, ORN A1a-ORN A2b
within sensillar subtype (but between ORN classes):
e.g. ORN A1a-ORN A1b, ORN A2a-ORN A2b
within ORN class:
e.g. ORN A1a-ORN A1a
Large basiconics
Thin basiconics
Small basiconics
Trichoids
Coeloconics
Amos/Lz, Atonal, etc
Sensillar type A precursor
Sensillar type B precursor
Rn, Dac, En, etc
Sensillar subtype A1 precursor
Sensillar subtype A2 precursor
Notch singling, Epigenetic modifier, Late TFs like Acj6, etc
ORN B1a
ORN A1a
ORN A1b
ORN A2a
ORN A2b
D
-log10(FDR)
log2FC(amos -/- vs WT)
log2FC(atonal -/- vs WT)
change
down
not significant
up
E
between sensillar types
within sensillar type (but between sensillar subtypes)
within sensillar subtype (but between ORN classes)
within ORN class
24h ORN
mid-pupal ORN
adult ORN
similarity
mean similarity
beats/sides
CSM genes
all genes
F
beats /sides
IgSF genes
CSM genes
24h APF
mid-pupal
adult

Figure S2. Characterization of *beat/side* expression in the published datasets of bulk antenna and single-cell RNA-seq of ORNs. Related to Figure 2.

(A) Dynamic *beats/side* expression in antennal tissues over development. Heatmap showing the temporal dynamic expression of *beats/sides* from 3rd instar larval antennal discs (larval), 8h APF pupal antennal discs, 40h APF antennae, and adult antennae. The color indicates the log-scaled relative expression values (base mean) of each gene at each stage from DESeq results.

(B) *beat/side* genes are differentially expressed across ORN classes at single-cell resolution. Each column is an annotated ORN class, and each dot represents the expression level of the row gene in the given ORN class, summarizing from the single-cell (24h APF, mid-pupal stage) or single-nucleus RNA-seq datasets (adult). The size of the dot denotes the fraction of "positive" cells in the given ORN class (log2(CPM+1) > 0.5), and the color denotes the mean expression of the positive cells.

(C) Hierarchical genetic programs control ORN lineage and glomerular targeting. A simplified model illustrating the ORN-ORN kinship. ORNs are housed in sensillar subtypes within each sensillar type, representing different genetic lineages. ORNs mapped to the same class are defined as "within ORN class", like ORN A1a and ORN A1a; ORNs of different classes but housed in the same sensillar subtype are defined as "within sensillar subtype", like ORN A1a and ORN A1b; ORNs from different sensillar subtypes but belonging to the same sensillar type, are defined as "within sensillar type", like ORN A1a and ORN A2a; and the furthest kinship is ORNs housed in distinct sensillar types, i.e., "between sensillar types", like ORN A1a and ORN B1a. Schematic was generated by BioRender. The antenna structure is reproduced from (Li et al., 2013).

(D) *beat/side* expression in the antenna is regulated by sensillar type-specification factors *amos* and *atonal.* Volcano plot showing the differentially expressed genes in *amos* mutant antennae compared with wild-type antennae (left panel) or *atonal* mutant antennae compared with wild-type antennae (right panel). Significantly downregulated *beat/side* genes are colored in blue, and significantly upregulated *beat/side* genes are colored in red. Significance is determined by FDR < 0.05 from EdgeR results. The horizontal dashed line in each plot is FDR = 0.05. Two vertical dashed lines in each plot are log2FC = -0.5 and 0.5, respectively. Gray dots are all other genes detected.

(E) Pairwise correlation between ORNs at three stages reveals the *beat/side* combinatorial expression is correlated with the ORN kinship. Top row in each stage: boxplot showing the similarity measured by Spearman's correlation between two cells from the indicated stage. The pairwise relation is categorized into four groups depending on the annotated ORN class and the corresponding sensillar type/subtype lineage. Bottom row in each stage: each dot is the mean similarity of the corresponding category in the top boxplot. The Spearman's correlation was calculated based on the expression of all beat/side genes, all CSM-encoding genes, or the whole transcriptome (all genes). P values are from Mann–Whitney U tests without multiple comparison adjustments. Figure 2E is reproduced here for comparison.

(F) *beat/side* combinatorial expression is more cell-population specific than pan-IgSF or pan-CSM genes across ORNs. Heatmap showing the Spearman's correlation of combinatorial gene expression between the row cell and the column cell across three developmental stages (24h APF, mid-pupal, and adult). The correlation was computed based on the combinatorial expression of *beat-side* genes, IgSF-encoding genes, or CSM-encoding genes. Cells are hierarchically clustered, as shown in the phylogeny tree in each heatmap. Correlation is shown as a spectrum from blue (-1) to red (1). The diagonal is the similarity of each cell to itself, and thus the correlation always equals 1.

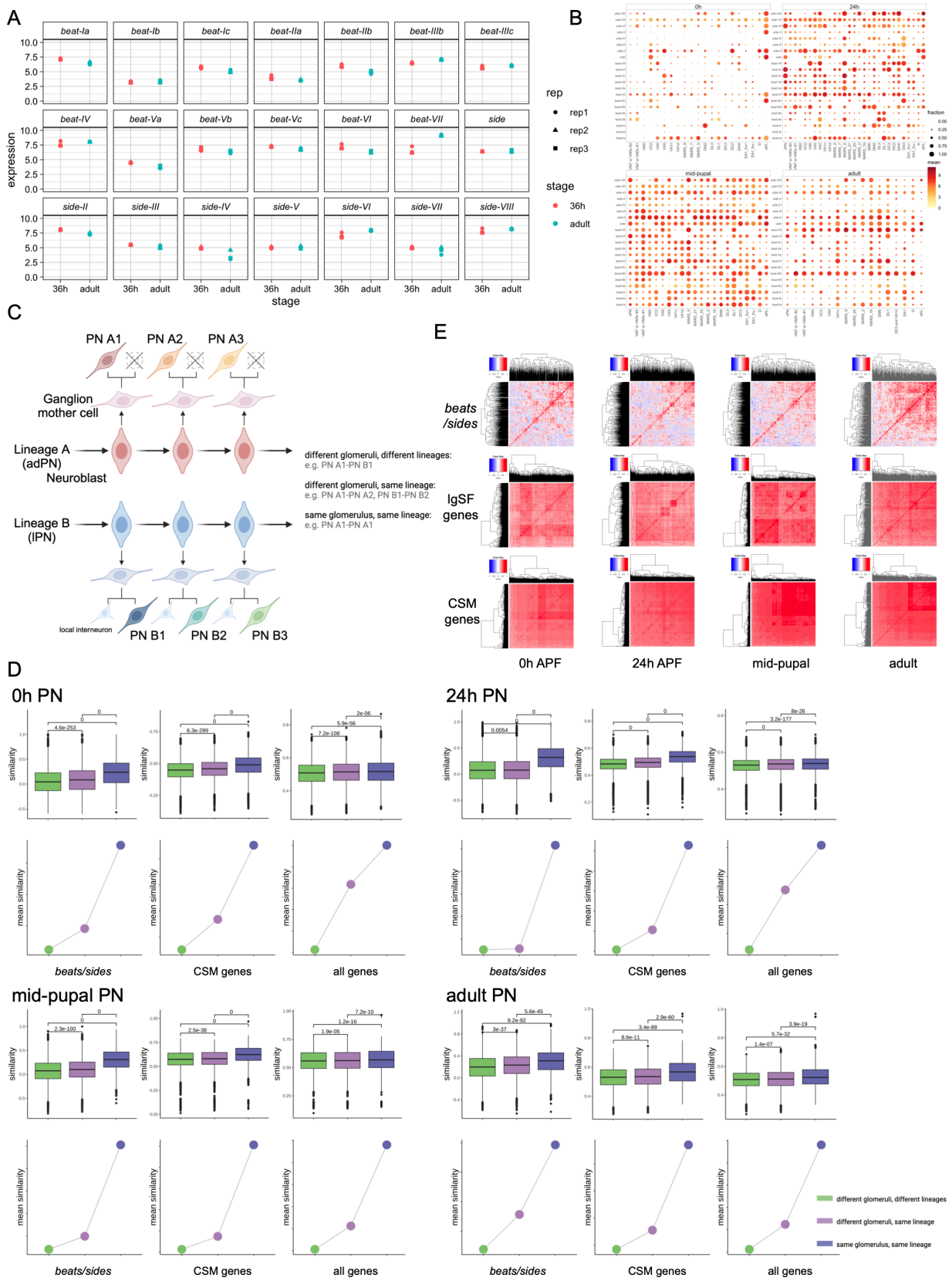
A
beat-Ia
beat-Ib
beat-Ic
beat-IIa
beat-IIb
beat-IIIb
beat-IIIc
beat-IV
beat-Va
beat-Vb
beat-Vc
beat-VI
beat-VII
side
side-II
side-III
side-IV
side-V
side-VI
side-VII
side-VIII
expression
stage
36h
adult
B
rep
rep1
rep2
rep3
stage
36h
adult
0h
24h
mid-pupal
adult
fraction
mean
C
PN A1
PN A2
PN A3
Ganglion mother cell
Lineage A (adPN) Neuroblast
Lineage B (lPN)
local interneuron
PN B1
PN B2
PN B3
different glomeruli, different lineages:
e.g. PN A1-PN B1
different glomeruli, same lineage:
e.g. PN A1-PN A2, PN B1-PN B2
same glomerulus, same lineage:
e.g. PN A1-PN A1
E
beats /sides
IgSF genes
CSM genes
0h APF
24h APF
mid-pupal
adult
D
0h PN
24h PN
mid-pupal PN
adult PN
similarity
mean similarity
beats/sides
CSM genes
all genes
different glomeruli, different lineages
different glomeruli, same lineage
same glomerulus, same lineage

874

875 **Figure S3. Characterization of *beat/side* expression in the published datasets of bulk and single-**
876 **cell RNA-seq of PNs. Related to Figure 3.**
877 **(A)** *beat/side* expression in bulk PNs over development. Point plots showing the *beat/side* expression in
878 the sorted bulk PNs from 36h APF and the adult stage. The shape of each point denotes the biological
879 replicate. The expression value is log2(CPM+1).
880 **(B)** *beat/side* genes are differentially expressed across PN classes at single-cell resolution. Each
881 column is an annotated PN class, and each dot represents the expression level of the row gene in the
882 given PN class, summarizing from the single-cell RNA-seq datasets. The size of the dot denotes the
883 fraction of "positive" cells in the given PN class (log2(CPM+1) > 0.5), and the color denotes the mean
884 expression of the positive cells. APL, anterior paired lateral neurons. APL and vPN clusters were not
885 used for the correlation analysis in D.
886 **(C)** Sequential genetic programs control PN lineage and glomerular targeting. We only used PNs
887 mapped to adPN and lPN lineage for correlation analysis. PNs from these two lineages are excitatory
888 and project to a single glomerulus, whereas the third lineage, vPN neurons, which were removed for
889 downstream analysis, are inhibitory GABAergic and can project to multiple glomeruli (Liang et al., 2013;
890 Marin et al., 2002). In the adPN lineage, one of the two post-mitotic neurons survives and develops into
891 a PN. In the lPN lineage, both post-mitotic neurons survive, one becoming a PN and the other
892 becoming a local interneuron (Lin et al., 2012; Lin et al., 2010). Schematic was generated by
893 BioRender.
894 **(D)** Pairwise correlation between PNs at four stages reveals the *beat/side* combinatorial expression is
895 correlated with the PN kinship. Top row in each stage: boxplot showing the similarity measured by
896 Spearman's correlation between two cells from the indicated stage. The pairwise relation is categorized
897 into three groups depending on the annotated PN class identity and the corresponding lineage identity.
898 Bottom row in each stage: each dot is the mean similarity of the corresponding category in the top
899 boxplot. The Spearman's correlation was calculated based on the expression of all beat/side genes, all
900 cell surface molecule (CSM)-encoding genes, or the whole transcriptome (all genes). P values are from
901 Mann–Whitney U tests without multiple comparison adjustments. Figure 3E is reproduced here for
902 comparison.
903 **(E)** *beat/side* combinatorial expression is more cell-population specific than pan-IgSF or pan-CSM
904 genes across PNs. Heatmap showing the Spearman's correlation of combinatorial gene expression
905 between the row cell and the column cell across four developmental stages (0h, 24h APF, mid-pupal,
906 and adult). The correlation was computed based on the combinatorial expression of *beat-side* genes,
907 IgSF-encoding genes, or cell surface molecule-encoding genes. Correlation is shown as a spectrum
908 from blue (-1) to red (1). Cells are hierarchically clustered, as shown in the phylogeny tree in each
909 heatmap. The diagonal is the similarity of each cell to itself, and thus the correlation always equals 1.
910

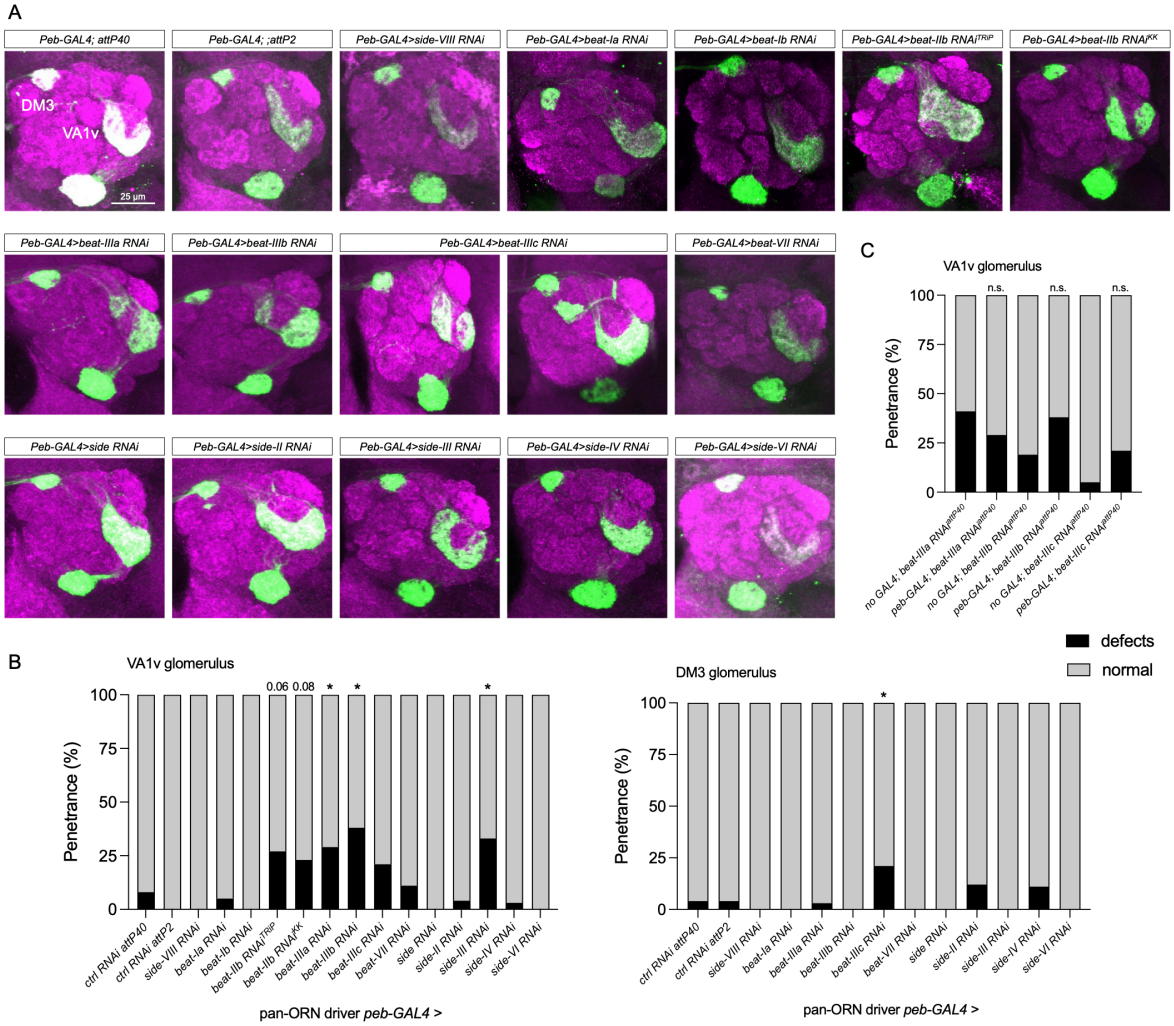

Figure S4. Perturbation of *beats/sides* in ORNs led to no or minor defects in glomerular organization. Related to Figure 4.

(A) Representative antennal lobes of controls and knockdowns of *beat/side* genes. Knockdown of *beat-IV* or *side-V* with this *peb-GAL4* driver caused lethality, and thus the data were missing.

(B) Quantification of the percentage of lobes showing glomerular defects of VA1v and DM3 glomeruli in each condition. N=20-50 antennal lobes examined. P values were determined by comparison to control groups. *, p<0.05.

(C) Quantification of the percentage of lobes showing glomerular defects of VA1v glomerulus of *beat-IIIa/b/c* perturbation with additional *RNAi* transgenic background controls. N=22-34 antennal lobes. n.s., not significant.

A

Peb-GAL4 + UAS-mCD8.GFP-P2A-sBRP.mStraw

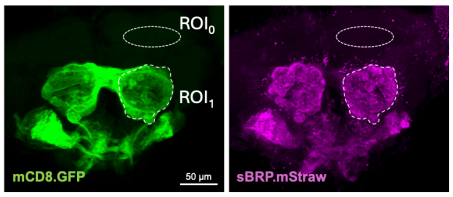

$$\text{Synaptic Density Index} = \frac{RFP_{ROI_1} - RFP_{ROI_0}}{GFP_{ROI_1} - GFP_{ROI_0}}$$

B

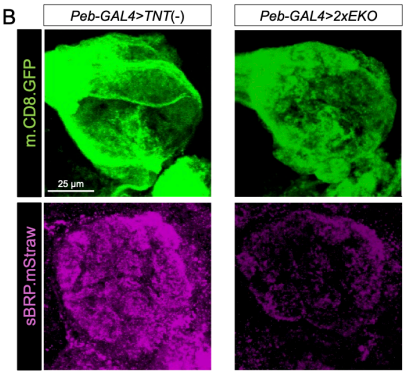

C

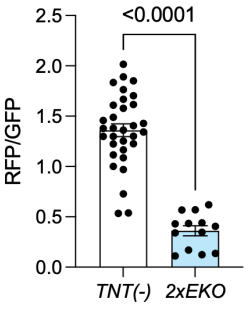

D

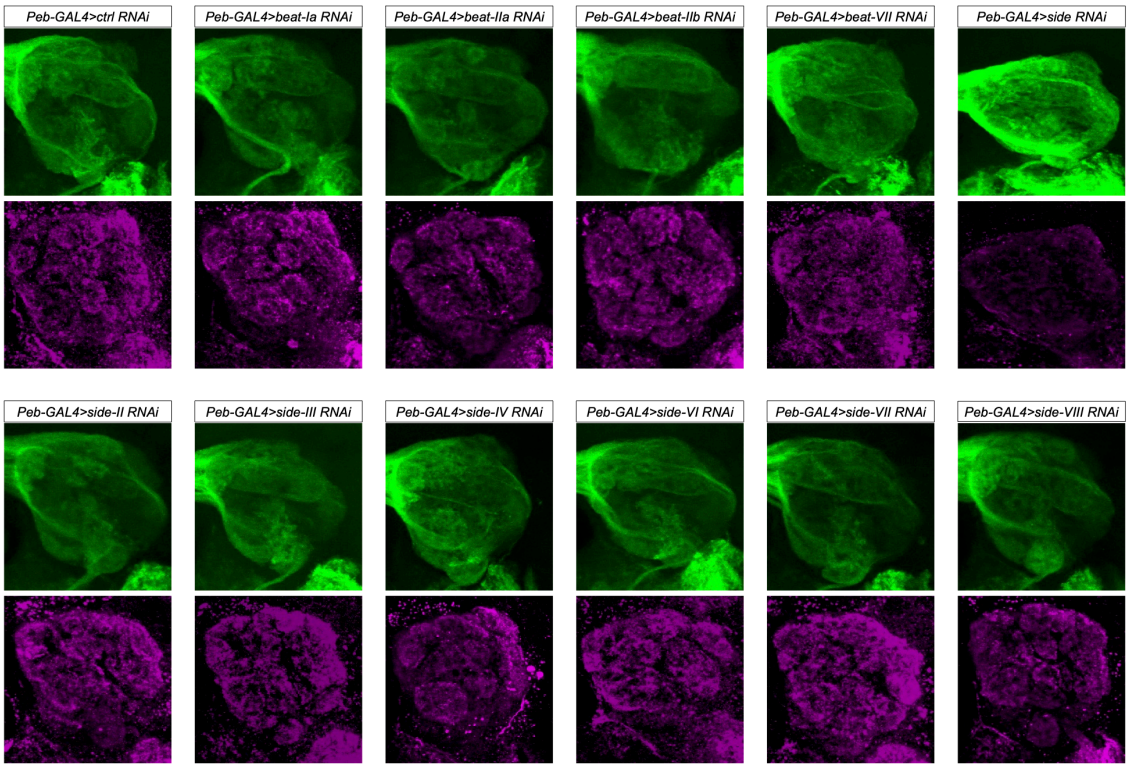

E

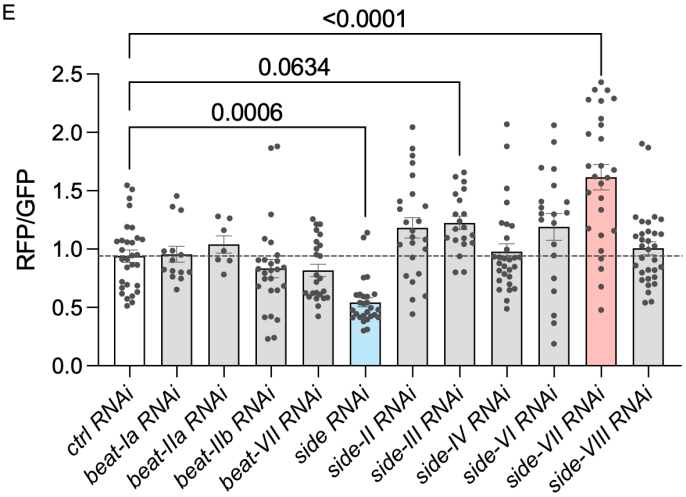

F

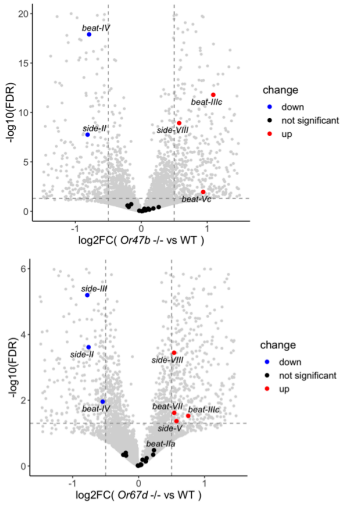

923

Figure S5. The effects of *beat/side* perturbation on synaptic density in ORNs. Related to Figure 4.

(A) Synaptic density is quantified by the ratio of the average fluorescence intensity of RFP and GFP in the region of interest, i.e., the antennal lobe. Synaptic active zone marker, short BRP protein.mStraw, and membrane marker, mCD8.GFP, are translated from the single transcript but localized in different subcellular regions (axon terminals vs general neurites).

(B) Representative antennal lobes showing the effects of blocking neuronal activity of ORNs on gross glomerular synaptic density, visualized by the membrane marker GFP and presynaptic marker RFP. Scale bar representing 25 μm also applies to each panel in (D).

(C) Quantification of (B). Each dot is a single antennal lobe. N = 43 and 13 antennal lobes, respectively. P-value from the unpaired t-test between groups is shown.

(D) Representative antennal lobes showing the effects of knockdown of *beats/sides* on gross glomerular synaptic density, visualized by the membrane marker GFP and presynaptic marker RFP. Knockdown of *beat-IV* or *side-V* with this *peb-GAL4* driver caused lethality, and thus the data were missing. There is little to no expression of *beat-Ib/c*, *beat-Va/b/c*, or *beat-VI* across ORNs; *beat-IIIa/b/c*, though expressed broadly, are orphans. These genes were not tested for their loss-of-function effects on synaptic density.

(E) Quantification of (D). Each dot is a single antennal lobe. N = 30, 14, 7, 26, 24, 27, 24, 20, 29, 20, 27, 32 antennal lobes, from left to right. Only P-values that are significant or near the edge from multiple comparisons post-ordinary-one-way ANOVA are shown. The dashed horizontal line indicates the mean values in the *ctrl RNAi* group. Groups of *ctrl RNAi* and *side RNAi* are the same samples as in Figure 4J.

(F) Volcano plot showing the differentially expressed genes in *Or47b* mutant antennae (top) and *Or67d* mutant antennae (bottom) compared with wild-type antennae. Significantly downregulated *beat/side* genes are colored in blue, and significantly upregulated *beat/side* genes are colored in red. Significance is determined by FDR<0.05 from DESeq2 results. The horizontal dashed line in each plot is FDR = 0.05. Two vertical dashed lines in each plot are log2FC = -0.5 and 0.5, respectively. Gray dots are all other genes detected. Data were reanalyzed from (Deanhardt et al., 2023).

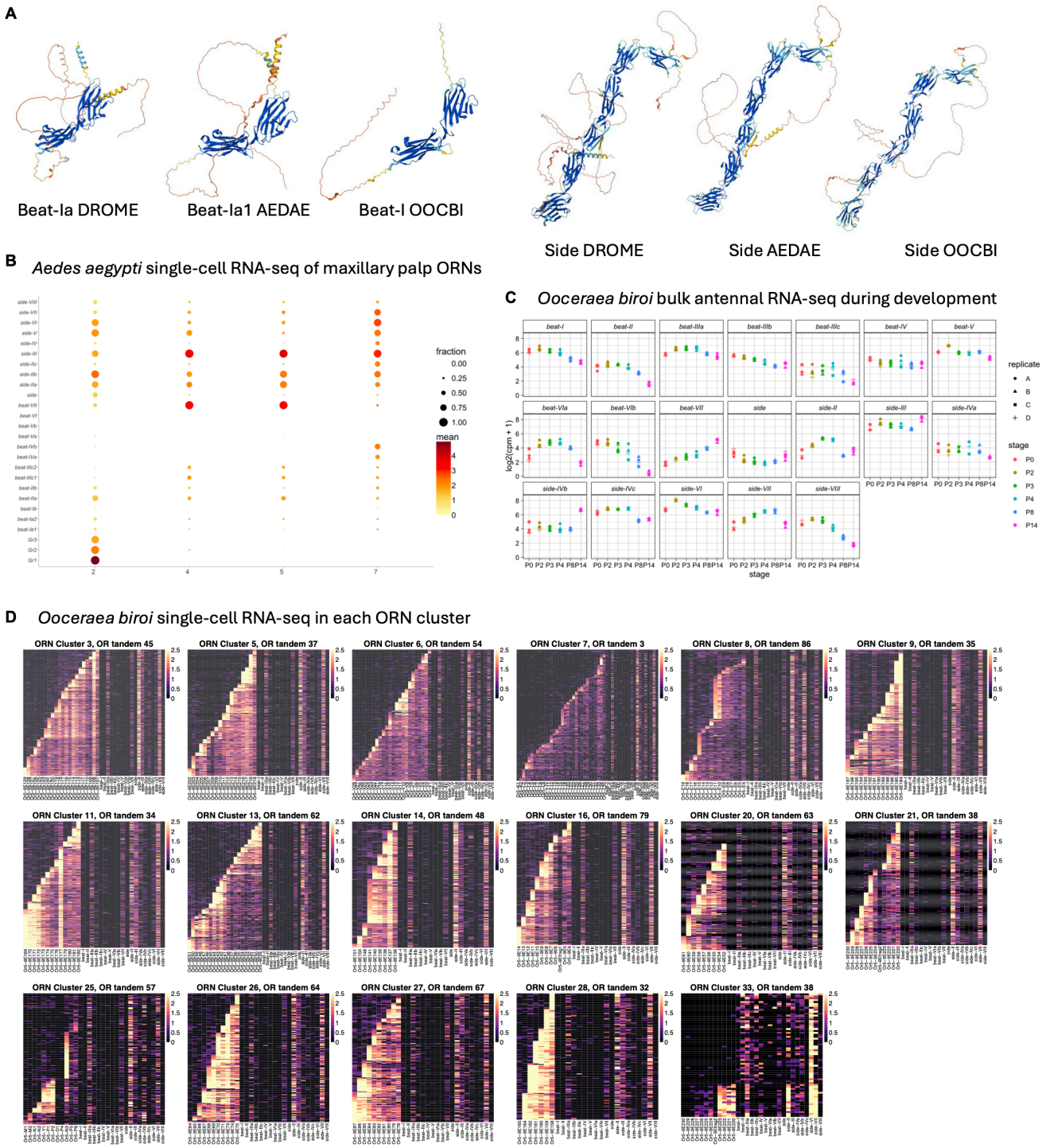

Figure S6. Additional analyses of *beat/sides* expression in mosquitoes and ants. Related to Figure 5.

(A) AlphaFold-predicted structures of example Beat and Side orthologs in fruit flies *Drosophila* melanogaster (DROME), yellow fever mosquitoes *Aedes aegypti* (AEDAE), and clonal raider ants *Ooceraea biroi* (OOCBI).

(B) Expression of *beats/sides* in the adult maxillary palp-housed ORN clusters of yellow mosquitoes based on the previously published single-cell RNA-seq data (Herre et al., 2022).

961 **(C)** Bulk RNA-seq showing the expression of *beats/sides* in developing antennal tissues of clonal raider
962 ants, reanalyzed from the data previously published (Ryba et al., 2020).
963 **(D)** Heatmap showing the expression of *beats/sides* and *OR* genes in all ORN clusters of clonal raider
964 ants that exhibit the ladder expression pattern of *OR* genes from 5' end to 3' end along a tandem,
965 based on the single-cell RNA-seq data from (Brahma et al., 2023). *OR* genes are ordered from 5' end
966 to 3' end in tandem in each cluster. Two clusters shown in Figure 5G are also reproduced here for
967 comparison. Data reanalyzed from (Brahma et al., 2023).
968

969 ## Materials and Methods

970 **Table 1. References and identifiers of the transgenic flies used in this study.**

Genotype	Reference	Identifier
hs-cre, vas-phiC31 (chrX)	(Diao et al., 2015)	BDSC 60299
Trojan-Gal4.0; Dr/TM3	(Diao et al., 2015)	BDSC 60301
Sp/CyO; Trojan-Gal4.0	(Diao et al., 2015)	BDSC 60302
Trojan-Gal4.1; Dr/TM3	(Diao et al., 2015)	BDSC 60304
Sp/CyO; Trojan-Gal4.1	(Diao et al., 2015)	BDSC 60305
Trojan-Gal4.2; Dr/TM3	(Diao et al., 2015)	BDSC 60307
Sp/CyO; Trojan-Gal4.2	(Diao et al., 2015)	BDSC 60308
10XUAS-IVS-myr.GFP attP40		BDSC 32198
10XUAS-IVS-myr.GFP attP2		BDSC 32197
beat-Ia-GAL4 [MI11181] chr2	This study	N.A.
beat-Ib-T2A-GAL4 [MI02527] chr2	This study	N.A.
beat-Ic-GAL4 [MI03347] chr2	This study	N.A.
beat-Ic-T2A-GAL4 [MI01467] chr2	This study	N.A.
beat-IIa-T2A-GAL4 [MI11485] chr3	(Lee et al., 2018)	BDSC 76215
beat-IIb-T2A-GAL4 [MI03102] chr3	This study	N.A.
beat-IIIa-T2A-GAL4 [MI14565] chr2	This study	N.A.
beat-IIIb-T2A-GAL4 [MI13179] chr2	(Lee et al., 2018)	BDSC 76227
beat-IIIc-T2A-GAL4 [MI03726] chr2	This study	N.A.
beat-IV-T2A-GAL4 [MI13984] chr3	This study	N.A.
beat-Va-T2A-GAL4 [MI00191] chr3	This study	N.A.
beat-Vc-T2A-GAL4 [MI08482] chr3	This study	N.A.
beat-VI-GAL4 [MI13252] chr3	This study	N.A.
beat-VII-GAL4 [MI07880] chr3	This study	N.A.
side-T2A-GAL4 [MI03741] chr3	This study	N.A.
side-II-T2A-GAL4 [MI07122] chr2	This study	N.A.
side-III-GAL4 [MI01491] chr3	This study	N.A.
side-IV-GAL4 [MI10049] chr3	This study	N.A.
side-V-GAL4 [MI04721] chr2	This study	N.A.
side-VI-T2A-GAL4 [MI03149] chr3	This study	N.A.
side-VII-GAL4 [MB10368] chr3		BDSC 29116
side-VIII-T2A-GAL4 [MI04810] chr2	This study	N.A.
ey-FLP (chrX)	(Newsome et al., 2000)	BDSC 5580
GH146-FLP (chr2)	(Hong et al., 2009)	BDSC 81291
UAS>STOP>mCD8.GFP (chr2)	(Hong et al., 2009)	BDSC 30125
UAS>STOP>mCD8.GFP (chr3)	(Hong et al., 2009)	BDSC 30032
peb-GAL4 (chrX)	(Sweeney et al., 2007)	N.A.
GH146-GAL4 (chrX)		BDSC 91812
UAS-Dcr (chrX)		BDSC 58726
Or42b-mCD8.GFP (chr2)		BDSC 52648

Or92a-mCD8.GFP (chr2)		BDSC 52646
Or47a-syt.GFP, Or47b-syt.GFP, Gr21a-syt.GFP (chr2)	Volkan lab stock	N.A.
UAS-Luc RNAi attP2		BDSC 31603
attP40		BDSC 36304
UAS-beat-Ia RNAi attP40		BDSC 64938
UAS-beat-Ib RNAi attP40		BDSC 57157
UAS-beat-IIa RNAi attP2		BDSC 28072
UAS-beat-IIb RNAi attP40		BDSC 57157
UAS-beat-IIb RNAi KK (chr2)		VDRC 104935
UAS-beat-IIIa RNAi attP40		BDSC 64526
UAS-beat-IIIb RNAi attP40		BDSC 56984
UAS-beat-IIIc RNAi attP40		BDSC 50941
UAS-beat-IV RNAi attP40		BDSC 56981
UAS-beat-VII RNAi attP40		BDSC 60056
UAS-side RNAi attP2		BDSC 50642
UAS-side-II RNAi KK (chr2)		VDRC 107512
UAS-side-III RNAi KK (chr2)		VDRC 103669
UAS-side-IV RNAi GD (chr2)		VDRC 16636
UAS-side-V RNAi attP40		BDSC 61953
UAS-side-VI RNAi KK (chr2)		VDRC 103456
UAS-side-VIII RNAi attP40		BDSC 62897
UAS-SynLight attP2	(Aimino et al., 2023)	BDSC 602367
UAS-TNT (-) (chr2)	(Sweeney et al., 1995)	BDSC 28840
2xUAS-EKO (chr2)	(White et al., 2001)	BDSC 40974

Table 2. References and identifiers of the sequencing datasets used in this study.

Dataset	Reference	Identifier
Antennal WT bulk RNA-seq of *Drosophila melanogaster*	(Barish et al., 2018)	GSE75986
PN WT bulk RNA-seq of *Drosophila melanogaster*	(Li et al., 2020b)	GSE140093
ORN single-cell RNA-seq of *Drosophila melanogaster*	(Li et al., 2020a; McLaughlin et al., 2021)	GSE162121 GSE143038
PN single-cell RNA-seq of *Drosophila melanogaster*	(Li et al., 2017a; Xie et al., 2021)	GSE161228 GSE100058
Amos mutant vs WT antennal RNA-seq of *Drosophila melanogaster*	(Mohapatra and Menuz, 2019)	PRJNA532415

Atonal mutant vs WT antennal RNA-seq of *Drosophila melanogaster*	(Menuz et al., 2014)	N.A.
Or mutant vs WT antennal RNA-seq of *Drosophila melanogaster*	(Deanhardt et al., 2023)	GSE179213
ORN single-cell RNA-seq of *Aedes aegypti*	(Herre et al., 2022)	GSE192978
ORN single-cell RNA-seq of *Ooceraea biroi*	(Brahma et al., 2023)	SRX21504666, SRX21504667

973

974 ***Drosophila* stocks and genetics**

975 Flies were raised in classic molasses media provided by Archon Scientific. Most crosses were
976 kept at room temperature (23 °C), except the RNAi experiments performed at 28 °C to
977 maximize the knockdown efficiency. For RNAi experiments, male and virgin female flies were
978 mixed at room temperature for three days to facilitate mating. Then flies were raised at a 28 °C
979 incubator until 5-7 days after eclosion before dissection. The transgenic *Drosophila*
980 *melanogaster* strains used in this study are listed in Table 1. BDSC, Bloomington Drosophila
981 Stock Center; VDRC, Vienna Drosophila Resource Center.

982

983 **Generating *T2A-GAL4* transgenic flies from *MiMIC* lines**

984 We used the *in vivo* genetic cross-based method (Diao et al., 2015) to swap the *T2A-GAL4*
985 construct with the *MiMIC* cassette. Briefly, by multiple crosses, the dual-recombinase (*hs-cre* +
986 *vas-phiC31*) helper component, the in-frame *T2A-GAL4* donor component, and the target
987 *MiMIC* locus in the genes of interest were introduced together into one parental animal, where
988 the *T2A-GAL4* donor sequence was excised out by Cre recombinase and inserted into the
989 *MiMIC* docking site by germline-expressed phiC31 integrase. When this parental animal was
990 crossed to the *UAS-myr.GFP* reporter line, the recombinant progeny would have GFP
991 expression driven by the *MiMIC-GAL4* if *T2A-GAL4* was inserted in the correct frame and
992 orientation. The recombinant was crossed with a double-balancer line to make a stable stock.
993 Specifically, we also found that the *T2A-GAL4* construct could be used in any 5' UTR-located
994 *MiMIC* sites in a frame-independent manner. In this case, the *GAL4* coding sequence with ATG
995 start codon in the 5' UTR would hijack the translation of the native gene as an upstream open
996 reading frame, and the *linker-T2A* sequence could be neglected. As the *GAL4* open reading
997 frame is within the whole transcript of the native gene, it is still expected to faithfully represent
998 the transcription levels and patterns of the native gene. We name the driver line *gene-GAL4* if
999 *GAL4* is within 5' UTR of the host gene (Table 1).

1000

1001 **Whole animal fluorescence imaging of *beat/side* expression**

1002 The whole animal fluorescence imaging was performed on an Olympus BX51WI upright scope
1003 equipped with a C11440-36U camera. Larvae and adults were killed by 70% ethanol first and
1004 mounted on slides without coverslips. Pupae were directly mounted on slides without
1005 coverslips. Larvae and pupae were dorsal side up, whereas adults were mounted with the

1006 lateral side up. Images were acquired under blue light and the GFP channel, with manually
1007 adjusted exposure time.

1008

1009 **Immunohistochemistry**

1010 Flies were first killed with 70% ethanol. Then, brains were dissected in PBST buffer (0.2%
1011 Triton X-100 in 1X PBS), fixed in 200 μL centrifuge tubes with 4% paraformaldehyde for 30
1012 minutes, followed by three 10-minute washes in PBST. Primary antibody mix (150 μL) was
1013 then added to the tubes, incubating brains on the orbital shaker at 4 °C overnight. Brains were
1014 washed three times for 20 minutes each with PBST at room temperature before secondary
1015 antibody staining. Secondary antibody mix (150 μL) was then added to the tubes, incubating
1016 brains on the orbital shaker at 4 °C overnight. Brains were washed three times for 20 minutes
1017 each with PBST at room temperature again before being mounted on the imaging slides.
1018 Natural goat serum (1%) was added to the primary and secondary antibody mix for blocking.
1019 The following primary antibodies with dilution ratio were used: rabbit anti-GFP (Invitrogen,
1020 1:1000), rat anti-Ncad (DSHB, 1:20), rabbit anti-DsRed (TaKaRa Bio, 1:250); the following
1021 secondary antibodies with dilution ratio were used: Alexa Fluor 488 goat anti-rabbit IgG
1022 (Invitrogen, 1:1000), Alexa Fluor 647 goat anti-rat IgG (Invitrogen, 1:200), Alexa Fluor Cy3 goat
1023 anti-rabbit IgG (Invitrogen, 1:200). Both primary and secondary antibody cocktails were diluted
1024 in PBST.

1025 Specifically, for Brp synaptic analysis, we only stained RFP mStraw and Ncad without staining
1026 GFP for two reasons. First, the transgenic mStraw fluorescence of the synaptic marker is very
1027 low and needs a very high laser power to detect the signal, while the natural GFP fluorescence
1028 is bright enough. Second, as we later normalized the RFP intensity by the GFP intensity as the
1029 proxy for synaptic density in the region of interest, no staining of GFP can reduce the variability
1030 introduced during immunohistochemistry.

1031

1032 **Confocal Imaging**

1033 To prepare brain samples for imaging, a mounting solution (Flouromount-G, SouthernBiotech)
1034 was added to the brains on the glass slide before the cover slip was mounted. Confocal
1035 images were acquired by either an Olympus Fluoview FV1000 microscope or a Zeiss 880
1036 microscope with a 40X or 60X objective lens. Brains were scanned through the Z-axis from the
1037 posterior side to the most anterior side of the antennal lobes. For *beat/side-GAL4*-based
1038 glomerular innervation analysis, imaging parameters varied between different *GAL4* drivers to
1039 highlight the lowly expressing glomeruli. For phenotypical determination, imaging parameters
1040 were kept consistent between experimental and control groups.

1041

1042 ***beat/side* glomerular expression pattern analysis of *beats/sides***

1043 For *ey-FLP* induced labeling of each *beat/side*-expressing ORN class, we found *ey-FLP*
1044 expression appears leaky in germline and crossing *ey-FLP* first with *UAS>STOP>mCD8.GFP*
1045 may lead to the removal of the *STOP* sequence constitutively and thereafter fail to restrict the
1046 GAL4-driven GFP expression solely in ORNs. To overcome this issue, we first crossed each
1047 *GAL4* driver line to the *ey-FLP* line and then crossed to *UAS>STOP>mCD8.GFP* reporter line.

1048 For *GH146-FLP* induced labeling of each *beat/side*-expressing PN class, each *GAL4* driver
1049 line can be directly crossed to the *GH146-FLP*; *UAS>STOP>mCD8.GFP* line. Only the results
1050 from female animals were reported in this study.

1051 As we aimed to determine the ORN or PN expression pattern of *beats/sides* in a binary
1052 manner, i.e., positive or negative, we didn't use the constant parameters to acquire the images
1053 for different *GAL4* driver lines. We adjusted the acquisition parameters in order to clearly show
1054 even lowly expressing glomeruli. After scanning each brain from the most posterior end to the
1055 most anterior end of the antennal lobe, we referred to the previously characterized glomerular
1056 map (Task et al., 2022) and manually determined the glomerular identity and the
1057 corresponding *beat/side* expression, assigning 0 to negative expression and 1 to positive
1058 expression. At least three brains were examined for each *GAL4* driver line. Notably, for the
1059 *GH146-FLP*-based labeling, we occasionally found inconsistent glomerular innervation
1060 patterns between individuals and even right and left lobes of the same brain (data not shown).
1061 This is likely due to the incomplete excision of the *STOP* cassette in a subset of PNs. As each
1062 glomerulus could be innervated by as few as one PN, it is possible that some glomeruli are not
1063 labeled in an antennal lobe. We thus determined these glomeruli to be positive if we observed
1064 the GFP signal for that glomerulus in two or more antennal lobes. The expression matrix,
1065 expression value (0,1) of each gene in each glomerulus, was then input to the downstream
1066 clustering analysis.

1067

1068 **Phenotype quantification**

1069 The measurement of the glomerular phenotype was determined by the proportion of antennal
1070 lobes showing morphological or positional abnormalities across all studied brains within each
1071 group, compared to the controls. The P-value was determined using the two-tailed Fisher's
1072 exact test, using the integrated features of the GraphPad Prism 9 software.

1073 To quantify synaptic density at the gross antennal lobe level, we first obtained the Z-stack of
1074 confocal sections by maximum projection. Then, we manually selected the regions of interest
1075 (ROI) according to the Ncad channel, which are the right and left antennal lobes. We also
1076 selected a control region in the dorsal part of the brain where the driver *peb-GAL4* has no
1077 expression. We then subtracted the average intensity of the RFP channel of the control region
1078 from that of the ROI. This is the adjusted mean RFP intensity of the ROI. We did the same
1079 thing to get the adjusted mean GFP intensity of the ROI. We finally calculated the ratio
1080 between the adjusted mean intensity of RFP and the adjusted mean intensity of GFP as the
1081 readout for each antennal lobe. An unpaired t-test or multiple comparisons post ordinary one-
1082 way ANOVA was used to compare the average RFP/GFP ratio between groups.

1083

1084 **Bulk tissue RNA-seq and single-cell RNA-seq analysis from previously published**
1085 **datasets for *Drosophila melanogaster***

1086 The publicly available datasets used are listed in Table 2. For bulk tissue RNA-seq datasets,
1087 the author-processed datasets (expression matrix and differentially expressed gene analysis
1088 by either EdgeR or DESeq) were directly used for customized analyses and visualization in
1089 this study. For single-cell RNA-seq datasets, the author-annotated expression matrices were
1090 directly used for similarity analysis (see details below).

1091

1092 **Pairwise similarity analysis for gene combinatorial expression in ORNs and PNs**

1093 The ORN single-cell RNA-seq dataset was first filtered to keep cells annotated to a single ORN
1094 class. Then, for cells in each stage, we extracted their *beat/side* expression profile, i.e., the
1095 vector of which each element is the expression value of each *beat/side* gene. We further
1096 filtered out the cells with zero expression for all *beat/side* genes. The remaining cells were
1097 used to calculate the expression correlation for *beat/side* genes and other gene combinations,
1098 e.g., IgSF-encoding genes or CSM-encoding genes. We first calculated the Spearman's
1099 correlation matrix for *beat/side* expression across the selected cells in each stage (Lv et al.,
1100 2022). Then, we assigned the kinship for each cell-cell pair based on the annotated
1101 ORN/glomerular identity, sensillum where they are housed, and the sensillar type (Couto et al.,
1102 2005; Fishilevich and Vosshall, 2005; Grabe et al., 2016; Marin et al., 2020; McLaughlin et al.,
1103 2021; Silbering et al., 2011; Task et al., 2022). Specifically, if two cells are annotated as the
1104 same ORN class, this pair is defined as "within ORN class"; if two cells are annotated as
1105 different ORN classes but both in the same sensillar subtype, this pair is defined as "within
1106 sensillar subtype"; if two cells are annotated as different ORN classes from different sensillar
1107 subtypes, but belong to the common sensillar type, this pair is defined as "within sensillar
1108 type"; if two cells are annotated as different ORN classes from different sensillar types, the pair
1109 is defined as "between sensillar types".

1110 The PN single-cell dataset was first filtered to keep cells annotated to a single PN class
1111 (excluding a small portion of anterior paired lateral (APL) neurons) and corresponding lineage
1112 identity. We only kept cells annotated to either adPN or lPN lineage (removed multiglomerular
1113 vPNs). Then, we extracted their *beat/side* expression vector for cells in each stage. We further
1114 filtered out the cells with zero expression for all *beat/side* genes. The remaining cells were
1115 used to analyze different gene combinations at the same stage. We first computed the
1116 Spearman's correlation matrix of *beat/side* expression across the selected cells in each stage.
1117 Then, we assigned the kinship for each cell-cell pair based on the annotated PN/glomerular
1118 identity and lineage identity. Specifically, if two cells are annotated as the same PN class, this
1119 pair is defined as "same glomerulus, same lineage"; if two cells are annotated as different PN
1120 classes but in the same PN lineage, this pair is defined as "different glomeruli, same lineage";
1121 if two cells are annotated as different PN classes from different PN lineages, this pair is defined
1122 as "different glomeruli, different lineages". Cell-cell pairs belonging to "same glomerulus,
1123 different lineages" were scarce and removed before statistical tests.

1124 We finally plotted the distribution of the correlation coefficient of each kinship category and
1125 compared the mean between the two categories using the Mann–Whitney U test. This analysis
1126 was expanded to the correlation of IgSF and CSM genes, randomly selected genes, or the
1127 whole transcriptome (all genes) at each stage. As the numbers of pairs (n) in each kinship
1128 category vary dramatically, we also randomly selected the same number of pairs in each
1129 kinship category. Then, we performed statistical tests on the resampled data and found the
1130 results to be true. Therefore, all related figures in this paper were plotted based on the original
1131 data without resampling.

1132 Shuffled control panels were calculated under the same pipeline as the abovementioned,
1133 except the annotations of each cell, ORN/PN class name, and corresponding lineage

information were shuffled. We shuffled 1000 times with different random seeds and plotted the average mean of each shuffling run.

A similar analysis was also applied to the *beat/side* genetic labeling results, where the binary expression matrices (with only 0 and 1) were used as the input. In this case, as each glomerulus represents the whole ORN/PN classes, we would not have the “within ORN class” or “same glomerulus, same lineage” category.

Ortholog identification and phylogenetic analysis of *beats* and *sides* in yellow fever mosquitoes and clonal raider ants

To identify the orthologs of *Drosophila melanogaster beat/side* genes in *Aedes aegypti* (yellow fever mosquitoes) and *Ooceraea biroi* (clonal raider ants), we used two ways to cross-validate the candidate list. For the biased way, we first queried the *Drosophila* genes one by one to get the putative orthologs in the other two species on www.orthodb.org (Tegenfeldt et al., 2025). Then, we queried the mosquito and ant genes to get the fruit fly orthologs. This reciprocal approach gave rise to a primary list of candidate *beats/sides* in mosquitoes and ants. For an unbiased way, we used the blastp tool on NCBI (https://blast.ncbi.nlm.nih.gov/Blast.cgi?PAGE=Proteins) to find the orthologous sequences encoded by the mosquito and ant genomes of *Drosophila* Beat-Ia and Side proteins. We applied additional filters, including protein size and AlphaFold-predicted structures (https://alphafold.ebi.ac.uk). We only kept candidates with comparable amino acid lengths to *Drosophila* homologs and similar protein structures (two Ig domains for Beats; five Ig domains and one fibronectin domain for Sides). This gave rise to a longer list of candidates. We compared these two lists and found that the first is contained in the second one. We then ran multiple sequence alignments of all Beat candidate and Side candidate proteins, together with the fruit fly ones, to build the phylogenetic trees, respectively, through the Clustal Omega program (Madeira et al., 2024) using the default parameters on https://www.uniprot.org.

Single-cell RNA-seq analysis of *beat/side* ortholog expression in the ORNs of yellow fever mosquitoes and clonal raider ants

Author-annotated single-cell RNA-seq datasets of *Aedes aegypti* and *Ooceraea biro* from two prior studies (Table 2) were directly used for downstream analyses and visualization. We extracted the mosquito and ant *beat/sides* genes from the original expression matrices. Based on the phylogenetic reconstruction described earlier, we renamed them to reflect their phylogenetic relationships with analogous genes in fruit flies (Table S1).

Statistics and code availability

R 4.3.1 and the necessary packages were used for all the abovementioned analyses and visualization. Statistical tests were performed with the built-in functions of R or through GraphPad Prism 9 software. The customized codes to replicate all illustrations and statistical graphs of this study will be uploaded to https://github.com/volkanlab.

1175 **Table S1. Orthologs of *beats/sides* in yellow fever mosquitoes *Aedes aegypti*, and clonal**
1176 **raider ants *Ooceraea biroi*.**

A. aegypti				
UniProt accession	**Gene ID**	**Length (aa)**	***D. mel* orthologs**	**New gene name**
A0A6I8TBN7	LOC5566816	403	Beat-Ia/Ib/Ic	*beat-Ia1*
A0A6I8U3J9	LOC5572937	329	Beat-Ia/Ib/Ic	*beat-Ia2*
A0A6I8TWI0	LOC110676758	293	Beat-Ia/Ib/Ic	*beat-Ib*
A0A6I8TXW0	LOC5566409	329	Beat-IIa/IIb	*beat-IIa*
A0A6I8TMU4	LOC5564746	296	Beat-IIa/IIb	*beat-IIb*
A0A1S4F2K6	LOC5575664	317	Beat-IIIa/IIIb/IIIc	*beat-IIIc1*
A0A6I8T6T3	LOC5575663	318	Beat-IIIa/IIIb/IIIc	*beat-IIIc2*
Q16T38	LOC5573307	323	Beat-IV	*beat-IVa*
A0A6I8T3Q5	LOC5564316	389	Beat-IV	*beat-IVb*
A0A6I8TBC6	LOC5571213	314	Beat-Va/Vb/Vc	*beat-Va*
A0A903UJK4	LOC5579262	303	Beat-Va/Vb/Vc	*beat-Vb*
A0A1S4G0B0	LOC5578571	372	Beat-VI	*beat-VI*
Q16UX7	LOC5572379	295	Beat-VII	*beat-VII*
A0A6I8TZ84	LOC5565349	824	Side	*side*
A0A6I8TMK3	LOC5571423	895	Side-II	*side-IIa*
A0A6I8T6R7	LOC5573643	975	Side-II	*side-IIb*
A0A6I8U3A5	LOC5572620	901	Side-II	*side-IIc*
A0A6I8TGL9	LOC5569913	1461	Side-III	*side-III*
A0A903V9A0	LOC5570293	996	Side-IV	*side-IV*
A0A6I8U5E3	LOC5566683	960	Side-V	*side-V*
A0A6I8T4J7	LOC5569257	979	Side-VI	*side-VI*
A0A903TT64	LOC5574581	929	Side-VII	*side-VII*
A0A6I8U0C6	LOC5576331	1062	Side-VIII	*side-VIII*
O. biroi				
UniProt accession	**Gene ID**	**Length (aa)**	***D. mel* orthologs**	**New gene name**
A0A026WLQ9	LOC105277757	303	Beat-Ia/Ib/Ic	*beat-I*
A0A3L8E3G8	LOC105281146	269	Beat-IIa/IIb	*beat-II*
A0A3L8D839	LOC105278748	296	Beat-IIIa/IIIb/IIIc	*beat-IIIa*
A0A3L8DA76	LOC105278750	296	Beat-IIIa/IIIb/IIIc	*beat-IIIb*
A0A3L8D610	LOC105284227	340	Beat-IIIa/IIIb/IIIc	*beat-IIIc*
A0A3L8DQF1	LOC105285218	269	Beat-IV	*beat-IV*
A0A3L8DGH2	LOC105275676	286	Beat-Va/Vb/Vc	*beat-V*

A0A3L8E4A2	LOC105279130	290	Beat-VI	*beat-VIa*
A0A3L8E121	LOC105282898	311	Beat-VI	*beat-VIb*
A0A3L8DUP0	LOC105278517	287	Beat-VII	*beat-VII*
A0A3L8D925	LOC105275893	795	Side	*side*
A0A026WW65	LOC105288222	806	Side-II	*side-II*
A0A026WJB3	LOC105278806	856	Side-III	*side-III*
A0A3L8E1Y0	LOC105274944	920	Side-IV	*side-IVa*
A0A026WV55	LOC105274945	836	Side-IV	*side-IVb*
A0A3L8D7Y1	LOC105275896	802	Side-IV	*side-IVc*
A0A3L8D540	LOC105286893	980	Side-VI	*side-VI*
A0A026X112	LOC105280531	941	Side-VII	*side-VII*
A0A3L8DGW7	LOC105287868	1010	Side-VIII	*side-VIII*

Author contributions

QD and PCV conceptualized the project and designed the experiments. QD did experiments, analyzed data, and prepared figures. Y-CDC, SO, QD, & LQR generated reagents. SO, RE, CY, and KMV helped with experiments. QD and PCV wrote and edited the manuscript.

Acknowledgement

The authors would also like to thank the Bloomington Drosophila Stock Center and the Vienna Drosophila Resource Center for providing the fruit fly strains and the Duke Light Microscopy Core Facility for technical support for imaging. The authors would also like to thank Drs. Claude Desplan and Richard S. Mann for sharing reagents, and members of the Volkan lab for discussions and comments on the manuscript. The authors particularly thank Allison Carson and Nick Manfred for assistance with the experiments. The authors also thank Drs. Hiroaki Matsunami, Corbin Jones, David McClay, and Amy Bejsovec for stimulating suggestions.

Funding

This study was supported by the U.S. National Science Foundation award 2006471 to PCV, National Institutes of Health NRSA F32EY032750 and NEI K99EY035757 to Y-CDC, and NINDS award NS070644 to RSM.

1199 ## References

1200 Aimino, M.A., J. Humenik, M.J. Parisi, J.C. Duhart, and T.J. Mosca. 2023. SynLight: a bicistronic
1201 strategy for simultaneous active zone and cell labeling in the Drosophila nervous system.
1202 *G3 (Bethesda)*. 13.
1203 Arguello, J.R., L. Abuin, J. Armida, K. Mika, P.C. Chai, and R. Benton. 2021. Targeted molecular
1204 profiling of rare olfactory sensory neurons identifies fate, wiring, and functional
1205 determinants. *Elife*. 10.
1206 Ashley, J., V. Sorrentino, M. Lobb-Rabe, S. Nagarkar-Jaiswal, L. Tan, S. Xu, Q. Xiao, K. Zinn, and R.A.
1207 Carrillo. 2019. Transsynaptic interactions between IgSF proteins DIP-alpha and Dpr10 are
1208 required for motor neuron targeting specificity. *Elife*. 8.
1209 Barish, S., S. Nuss, I. Strunilin, S. Bao, S. Mukherjee, C.D. Jones, and P.C. Volkan. 2018.
1210 Combinations of DIPs and Dprs control organization of olfactory receptor neuron terminals
1211 in Drosophila. *PLoS Genet*. 14:e1007560.
1212 Barish, S., and P.C. Volkan. 2015. Mechanisms of olfactory receptor neuron specification in
1213 Drosophila. *Wiley Interdiscip Rev Dev Biol*. 4:609-621.
1214 Blagburn, J.M. 2008. Engrailed expression in subsets of adult Drosophila sensory neurons: an
1215 enhancer-trap study. *Invert Neurosci*. 8:133-146.
1216 Brahma, A., D.D. Frank, P.D.H. Pastor, P.K. Piekarski, W. Wang, J.D. Luo, T.S. Carroll, and D.J.C.
1217 Kronauer. 2023. Transcriptional and post-transcriptional control of odorant receptor choice
1218 in ants. *Curr Biol*. 33:5456-5466 e5455.
1219 Brochtrup, A., and T. Hummel. 2011. Olfactory map formation in the Drosophila brain: genetic
1220 specificity and neuronal variability. *Curr Opin Neurobiol*. 21:85-92.
1221 Brovero, S.G., J.C. Fortier, H. Hu, P.C. Lovejoy, N.R. Newell, C.M. Palmateer, R.Y. Tzeng, P.T. Lee, K.
1222 Zinn, and M.N. Arbeitman. 2021. Investigation of Drosophila fruitless neurons that express
1223 Dpr/DIP cell adhesion molecules. *Elife*. 10.
1224 Carrier, Y., L. Quintana Rio, N. Formicola, V. de Sousa-Xavier, M. Tabet, Y.D. Chen, A.H. Ali, M.
1225 Wislez, L. Orts, A. Borst, and F. Pinto-Teixeira. 2025. Biased cell adhesion organizes the
1226 Drosophila visual motion integration circuit. *Dev Cell*. 60:762-779 e767.
1227 Carrillo, R.A., E. Ozkan, K.P. Menon, S. Nagarkar-Jaiswal, P.T. Lee, M. Jeon, M.E. Birnbaum, H.J.
1228 Bellen, K.C. Garcia, and K. Zinn. 2015. Control of Synaptic Connectivity by a Network of
1229 Drosophila IgSF Cell Surface Proteins. *Cell*. 163:1770-1782.
1230 Chai, P.C., S. Cruchet, L. Wigger, and R. Benton. 2019. Sensory neuron lineage mapping and
1231 manipulation in the Drosophila olfactory system. *Nat Commun*. 10:643.
1232 Cheng, S., J. Ashley, J.D. Kurleto, M. Lobb-Rabe, Y.J. Park, R.A. Carrillo, and E. Ozkan. 2019a.
1233 Molecular basis of synaptic specificity by immunoglobulin superfamily receptors in
1234 Drosophila. *Elife*. 8.
1235 Cheng, S., Y. Park, J.D. Kurleto, M. Jeon, K. Zinn, J.W. Thornton, and E. Ozkan. 2019b. Family of
1236 neural wiring receptors in bilaterians defined by phylogenetic, biochemical, and structural
1237 evidence. *Proc Natl Acad Sci U S A*. 116:9837-9842.
1238 Cosmanescu, F., P.S. Katsamba, A.P. Sergeeva, G. Ahlsen, S.D. Patel, J.J. Brewer, L. Tan, S. Xu, Q.
1239 Xiao, S. Nagarkar-Jaiswal, A. Nern, H.J. Bellen, S.L. Zipursky, B. Honig, and L. Shapiro. 2018.
1240 Neuron-Subtype-Specific Expression, Interaction Affinities, and Specificity Determinants
1241 of DIP/Dpr Cell Recognition Proteins. *Neuron*. 100:1385-1400 e1386.

1242 Courgeon, M., and C. Desplan. 2019. Coordination between stochastic and deterministic
1243 specification in the Drosophila visual system. *Science*. 366.
1244 Couto, A., M. Alenius, and B.J. Dickson. 2005. Molecular, anatomical, and functional organization
1245 of the Drosophila olfactory system. *Curr Biol*. 15:1535-1547.
1246 de Jong, S., J.A. Cavallo, C.D. Rios, H.A. Dworak, and H. Sink. 2005. Target recognition and
1247 synaptogenesis by motor axons: responses to the sidestep protein. *Int J Dev Neurosci*.
1248 23:397-410.
1249 Deanhardt, B., Q. Duan, C. Du, C. Soeder, A. Morlote, D. Garg, A. Saha, C.D. Jones, and P.C.
1250 Volkan. 2023. Social experience and pheromone receptor activity reprogram gene
1251 expression in sensory neurons. *G3 (Bethesda)*. 13.
1252 Diao, F., H. Ironfield, H. Luan, F. Diao, W.C. Shropshire, J. Ewer, E. Marr, C.J. Potter, M. Landgraf,
1253 and B.H. White. 2015. Plug-and-play genetic access to drosophila cell types using
1254 exchangeable exon cassettes. *Cell Rep*. 10:1410-1421.
1255 Dombrovski, M., Y. Zang, G. Frighetto, A. Vaccari, H. Jang, P.S. Mirshahidi, F. Xie, P. Sanfilippo, B.W.
1256 Hina, A. Rehan, R.H. Hussein, P.S. Mirshahidi, C. Lee, A. Morris, M.A. Frye, C.R. von Reyn,
1257 Y.Z. Kurmangaliyev, G.M. Card, and S.L. Zipursky. 2025. Molecular gradients shape synaptic
1258 specificity of a visuomotor transformation. *Nature*.
1259 Duan, Q., R. Estrella, A. Carson, Y. Chen, and P.C. Volkan. 2023. The effect of Drosophila attP40
1260 background on the glomerular organization of Or47b olfactory receptor neurons. *G3*
1261 *(Bethesda)*.
1262 Duan, Q., and P.C. Volkan. 2020. Ant Olfaction: Smells Like an Insect, Develops Like a Mammal.
1263 *Curr Biol*. 30:R950-R952.
1264 Endo, K., T. Aoki, Y. Yoda, K. Kimura, and C. Hama. 2007. Notch signal organizes the Drosophila
1265 olfactory circuitry by diversifying the sensory neuronal lineages. *Nat Neurosci*. 10:153-160.
1266 Fambrough, D., and C.S. Goodman. 1996. The Drosophila beaten path gene encodes a novel
1267 secreted protein that regulates defasciculation at motor axon choice points. *Cell*. 87:1049-
1268 1058.
1269 Fishilevich, E., and L.B. Vosshall. 2005. Genetic and functional subdivision of the Drosophila
1270 antennal lobe. *Curr Biol*. 15:1548-1553.
1271 Goulding, S.E., P. zur Lage, and A.P. Jarman. 2000. amos, a proneural gene for Drosophila olfactory
1272 sense organs that is regulated by lozenge. *Neuron*. 25:69-78.
1273 Goyal, G., A. Zierau, M. Lattemann, B. Bergkirchner, D. Javorski, R. Kaur, and T. Hummel. 2019.
1274 Inter-axonal recognition organizes Drosophila olfactory map formation. *Sci Rep*. 9:11554.
1275 Grabe, V., A. Baschwitz, H.K.M. Dweck, S. Lavista-Llanos, B.S. Hansson, and S. Sachse. 2016.
1276 Elucidating the Neuronal Architecture of Olfactory Glomeruli in the Drosophila Antennal
1277 Lobe. *Cell Rep*. 16:3401-3413.
1278 Gupta, B.P., G.V. Flores, U. Banerjee, and V. Rodrigues. 1998. Patterning an epidermal field:
1279 Drosophila lozenge, a member of the AML-1/Runt family of transcription factors, specifies
1280 olfactory sense organ type in a dose-dependent manner. *Dev Biol*. 203:400-411.
1281 Gupta, B.P., and V. Rodrigues. 1997. Atonal is a proneural gene for a subset of olfactory sense
1282 organs in Drosophila. *Genes Cells*. 2:225-233.
1283 Hattori, D., E. Demir, H.W. Kim, E. Viragh, S.L. Zipursky, and B.J. Dickson. 2007. Dscam diversity is
1284 essential for neuronal wiring and self-recognition. *Nature*. 449:223-227.

1285 Herre, M., O.V. Goldman, T.C. Lu, G. Caballero-Vidal, Y. Qi, Z.N. Gilbert, Z. Gong, T. Morita, S.
1286 Rahiel, M. Ghaninia, R. Ignell, B.J. Matthews, H. Li, L.B. Vosshall, and M.A. Younger. 2022.
1287 Non-canonical odor coding in the mosquito. *Cell*. 185:3104-3123 e3128.
1288 Heymann, C., C. Paul, N. Huang, J.C. Kinold, A.C. Dietrich, and H. Aberle. 2022. Molecular insights
1289 into the axon guidance molecules Sidestep and Beaten path. *Frontiers in Physiology*. 13.
1290 Hong, W., and L. Luo. 2014. Genetic control of wiring specificity in the fly olfactory system.
1291 *Genetics*. 196:17-29.
1292 Hong, W., T.J. Mosca, and L. Luo. 2012. Teneurins instruct synaptic partner matching in an
1293 olfactory map. *Nature*. 484:201-207.
1294 Hong, W., H. Zhu, C.J. Potter, G. Barsh, M. Kurusu, K. Zinn, and L. Luo. 2009. Leucine-rich repeat
1295 transmembrane proteins instruct discrete dendrite targeting in an olfactory map. *Nat*
1296 *Neurosci*. 12:1542-1550.
1297 Honig, B., and L. Shapiro. 2020. Adhesion Protein Structure, Molecular Affinities, and Principles of
1298 Cell-Cell Recognition. *Cell*. 181:520-535.
1299 Hummel, T., M.L. Vasconcelos, J.C. Clemens, Y. Fishilevich, L.B. Vosshall, and S.L. Zipursky. 2003.
1300 Axonal targeting of olfactory receptor neurons in Drosophila is controlled by Dscam.
1301 *Neuron*. 37:221-231.
1302 Hummel, T., and S.L. Zipursky. 2004. Afferent induction of olfactory glomeruli requires N-cadherin.
1303 *Neuron*. 42:77-88.
1304 Imai, T., H. Sakano, and L.B. Vosshall. 2010. Topographic mapping--the olfactory system. *Cold*
1305 *Spring Harb Perspect Biol*. 2:a001776.
1306 Jefferis, G.S., and T. Hummel. 2006. Wiring specificity in the olfactory system. *Semin Cell Dev Biol*.
1307 17:50-65.
1308 Jefferis, G.S., E.C. Marin, R.F. Stocker, and L. Luo. 2001. Target neuron prespecification in the
1309 olfactory map of Drosophila. *Nature*. 414:204-208.
1310 Jumper, J., R. Evans, A. Pritzel, T. Green, M. Figurnov, O. Ronneberger, K. Tunyasuvunakool, R.
1311 Bates, A. Zidek, A. Potapenko, A. Bridgland, C. Meyer, S.A.A. Kohl, A.J. Ballard, A. Cowie, B.
1312 Romera-Paredes, S. Nikolov, R. Jain, J. Adler, T. Back, S. Petersen, D. Reiman, E. Clancy, M.
1313 Zielinski, M. Steinegger, M. Pacholska, T. Berghammer, S. Bodenstein, D. Silver, O. Vinyals,
1314 A.W. Senior, K. Kavukcuoglu, P. Kohli, and D. Hassabis. 2021. Highly accurate protein
1315 structure prediction with AlphaFold. *Nature*. 596:583-589.
1316 Kinold, J.C., M. Brenner, and H. Aberle. 2021. Misregulation of Drosophila Sidestep Leads to
1317 Uncontrolled Wiring of the Adult Neuromuscular System and Severe Locomotion Defects.
1318 *Front Neural Circuits*. 15:658791.
1319 Kinold, J.C., C. Pfarr, and H. Aberle. 2018. Sidestep-induced neuromuscular miswiring causes
1320 severe locomotion defects in Drosophila larvae. *Development*. 145.
1321 Komiyama, T., J.R. Carlson, and L. Luo. 2004. Olfactory receptor neuron axon targeting: intrinsic
1322 transcriptional control and hierarchical interactions. *Nat Neurosci*. 7:819-825.
1323 Komiyama, T., W.A. Johnson, L. Luo, and G.S. Jefferis. 2003. From lineage to wiring specificity. POU
1324 domain transcription factors control precise connections of Drosophila olfactory
1325 projection neurons. *Cell*. 112:157-167.
1326 Lee, P.T., J. Zirin, O. Kanca, W.W. Lin, K.L. Schulze, D. Li-Kroeger, R. Tao, C. Devereaux, Y. Hu, V.
1327 Chung, Y. Fang, Y. He, H. Pan, M. Ge, Z. Zuo, B.E. Housden, S.E. Mohr, S. Yamamoto, R.W.

1328 Levis, A.C. Spradling, N. Perrimon, and H.J. Bellen. 2018. A gene-specific T2A-GAL4 library
1329 for Drosophila. *Elife*. 7.
1330 Li, H., F. Horns, B. Wu, Q. Xie, J. Li, T. Li, D.J. Luginbuhl, S.R. Quake, and L. Luo. 2017a. Classifying
1331 Drosophila Olfactory Projection Neuron Subtypes by Single-Cell RNA Sequencing. *Cell*.
1332 171:1206-1220 e1222.
1333 Li, H., T. Li, F. Horns, J. Li, Q. Xie, C. Xu, B. Wu, J.M. Kebschull, C.N. McLaughlin, S.S. Kolluru, R.C.
1334 Jones, D. Vacek, A. Xie, D.J. Luginbuhl, S.R. Quake, and L. Luo. 2020a. Single-Cell
1335 Transcriptomes Reveal Diverse Regulatory Strategies for Olfactory Receptor Expression
1336 and Axon Targeting. *Curr Biol*. 30:1189-1198 e1185.
1337 Li, H., S.A. Shuster, J. Li, and L. Luo. 2018. Linking neuronal lineage and wiring specificity. *Neural*
1338 *Dev*. 13:5.
1339 Li, H., A. Watson, A. Olechwier, M. Anaya, S.K. Sorooshyari, D.P. Harnett, H.P. Lee, J. Vielmetter,
1340 M.A. Fares, K.C. Garcia, E. Ozkan, J.P. Labrador, and K. Zinn. 2017b. Deconstruction of the
1341 beaten Path-Sidestep interaction network provides insights into neuromuscular system
1342 development. *Elife*. 6.
1343 Li, J., S. Han, H. Li, N.D. Udeshi, T. Svinkina, D.R. Mani, C. Xu, R. Guajardo, Q. Xie, T. Li, D.J.
1344 Luginbuhl, B. Wu, C.N. McLaughlin, A. Xie, P. Kaewsapsak, S.R. Quake, S.A. Carr, A.Y. Ting,
1345 and L. Luo. 2020b. Cell-Surface Proteomic Profiling in the Fly Brain Uncovers Wiring
1346 Regulators. *Cell*. 180:373-386 e315.
1347 Li, Q., S. Barish, S. Okuwa, A. Maciejewski, A.T. Brandt, D. Reinhold, C.D. Jones, and P.C. Volkan.
1348 2016. A Functionally Conserved Gene Regulatory Network Module Governing Olfactory
1349 Neuron Diversity. *PLoS Genet*. 12:e1005780.
1350 Li, Q., T.S. Ha, S. Okuwa, Y. Wang, Q. Wang, S.S. Millard, D.P. Smith, and P.C. Volkan. 2013.
1351 Combinatorial rules of precursor specification underlying olfactory neuron diversity. *Curr*
1352 *Biol*. 23:2481-2490.
1353 Li, Z., C. Lyu, C. Xu, Y. Hu, D.J. Luginbuhl, A.B. Caspi-Lebovic, J.M. Priest, E. Ozkan, and L. Luo.
1354 2025. Repulsive interactions instruct synaptic partner matching in an olfactory circuit.
1355 *bioRxiv*.
1356 Liang, L., Y. Li, C.J. Potter, O. Yizhar, K. Deisseroth, R.W. Tsien, and L. Luo. 2013. GABAergic
1357 projection neurons route selective olfactory inputs to specific higher-order neurons.
1358 *Neuron*. 79:917-931.
1359 Lin, S., C.F. Kao, H.H. Yu, Y. Huang, and T. Lee. 2012. Lineage analysis of Drosophila lateral
1360 antennal lobe neurons reveals notch-dependent binary temporal fate decisions. *PLoS Biol*.
1361 10:e1001425.
1362 Lin, S., S.L. Lai, H.H. Yu, T. Chihara, L. Luo, and T. Lee. 2010. Lineage-specific effects of
1363 Notch/Numb signaling in post-embryonic development of the Drosophila brain.
1364 *Development*. 137:43-51.
1365 Lobb-Rabe, M., W.I. Nawrocka, R. Zhang, J. Ashley, R.A. Carrillo, and E. Ozkan. 2024. Neuronal
1366 Wiring Receptors Dprs and DIPs Are GPI Anchored and This Modification Contributes to
1367 Their Cell Surface Organization. *eNeuro*. 11.
1368 Lv, X., S. Li, J. Li, X.Y. Yu, X. Ge, B. Li, S. Hu, Y. Lin, S. Zhang, J. Yang, X. Zhang, J. Yan, A.L. Joyner, H.
1369 Shi, Q. Wu, and S.H. Shi. 2022. Patterned cPCDH expression regulates the fine organization
1370 of the neocortex. *Nature*. 612:503-511.

1371 Lyu, C., Z. Li, C. Xu, J. Kalai, and L. Luo. 2025. Rewiring an olfactory circuit by altering the
1372 combinatorial code of cell-surface proteins. *Res Sq*.
1373 Madeira, F., N. Madhusoodanan, J. Lee, A. Eusebi, A. Niewielska, A.R.N. Tivey, R. Lopez, and S.
1374 Butcher. 2024. The EMBL-EBI Job Dispatcher sequence analysis tools framework in 2024.
1375 *Nucleic Acids Res*. 52:W521-W525.
1376 Marin, E.C., L. Buld, M. Theiss, T. Sarkissian, R.J.V. Roberts, R. Turnbull, I.F.M. Tamimi, M.W.
1377 Pleijzier, W.J. Laursen, N. Drummond, P. Schlegel, A.S. Bates, F. Li, M. Landgraf, M. Costa,
1378 D.D. Bock, P.A. Garrity, and G. Jefferis. 2020. Connectomics Analysis Reveals First-,
1379 Second-, and Third-Order Thermosensory and Hygrosensory Neurons in the Adult
1380 Drosophila Brain. *Curr Biol*. 30:3167-3182 e3164.
1381 Marin, E.C., G.S. Jefferis, T. Komiyama, H. Zhu, and L. Luo. 2002. Representation of the glomerular
1382 olfactory map in the Drosophila brain. *Cell*. 109:243-255.
1383 Marin, E.C., R.J. Watts, N.K. Tanaka, K. Ito, and L. Luo. 2005. Developmentally programmed
1384 remodeling of the Drosophila olfactory circuit. *Development*. 132:725-737.
1385 McLaughlin, C.N., M. Brbic, Q. Xie, T. Li, F. Horns, S.S. Kolluru, J.M. Kebschull, D. Vacek, A. Xie, J. Li,
1386 R.C. Jones, J. Leskovec, S.R. Quake, L. Luo, and H. Li. 2021. Single-cell transcriptomes of
1387 developing and adult olfactory receptor neurons in Drosophila. *Elife*. 10.
1388 Menon, K.P., V. Kulkarni, S.Y. Takemura, M. Anaya, and K. Zinn. 2019. Interactions between Dpr11
1389 and DIP-gamma control selection of amacrine neurons in Drosophila color vision circuits.
1390 *Elife*. 8.
1391 Menuz, K., N.K. Larter, J. Park, and J.R. Carlson. 2014. An RNA-seq screen of the Drosophila
1392 antenna identifies a transporter necessary for ammonia detection. *PLoS Genet*.
1393 10:e1004810.
1394 Mohapatra, P., and K. Menuz. 2019. Molecular Profiling of the Drosophila Antenna Reveals
1395 Conserved Genes Underlying Olfaction in Insects. *G3 (Bethesda)*. 9:3753-3771.
1396 Morano, N.C., D.H. Lopez, H. Meltzer, A.P. Sergeeva, P.S. Katsamba, K.D. Rostam, H.P. Gupta, J.E.
1397 Becker, B. Bornstein, F. Cosmanescu, O. Schuldiner, B. Honig, R.S. Mann, and L. Shapiro.
1398 2025. Members of the DIP and Dpr adhesion protein families use cis inhibition to shape
1399 neural development in Drosophila. *PLoS Biol*. 23:e3003030.
1400 Mosca, T.J., and L. Luo. 2014. Synaptic organization of the Drosophila antennal lobe and its
1401 regulation by the Teneurins. *Elife*. 3:e03726.
1402 Newsome, T.P., B. Asling, and B.J. Dickson. 2000. Analysis of Drosophila photoreceptor axon
1403 guidance in eye-specific mosaics. *Development*. 127:851-860.
1404 Osaka, J., A. Ishii, X. Wang, R. Iwanaga, H. Kawamura, S. Akino, A. Sugie, S. Hakeda-Suzuki, and T.
1405 Suzuki. 2024. Complex formation of immunoglobulin superfamily molecules Side-IV and
1406 Beat-IIb regulates synaptic specificity. *Cell Rep*. 43:113798.
1407 Özkan, E., R.A. Carrillo, C.L. Eastman, R. Weiszmann, D. Waghray, K.G. Johnson, K. Zinn, S.E.
1408 Celniker, and K.C. Garcia. 2013. An extracellular interactome of immunoglobulin and LRR
1409 proteins reveals receptor-ligand networks. *Cell*. 154:228-239.
1410 Pipes, G.C., Q. Lin, S.E. Riley, and C.S. Goodman. 2001. The Beat generation: a multigene family
1411 encoding IgSF proteins related to the Beat axon guidance molecule in Drosophila.
1412 *Development*. 128:4545-4552.
1413 Rodrigues, V., and T. Hummel. 2008. Development of the Drosophila olfactory system. *Adv Exp*
1414 *Med Biol*. 628:82-101.

1415 Royet, J., and R. Finkelstein. 1997. Establishing primordia in the Drosophila eye-antennal imaginal
1416 disc: the roles of decapentaplegic, wingless and hedgehog. *Development*. 124:4793-4800.
1417 Ryba, A.R., S.K. McKenzie, L. Olivos-Cisneros, E.J. Clowney, P.M. Pires, and D.J.C. Kronauer. 2020.
1418 Comparative Development of the Ant Chemosensory System. *Curr Biol*. 30:3223-3230
1419 e3224.
1420 Sanes, J.R., and S.L. Zipursky. 2020. Synaptic Specificity, Recognition Molecules, and Assembly of
1421 Neural Circuits. *Cell*. 181:1434-1435.
1422 Siebert, M., D. Banovic, B. Goellner, and H. Aberle. 2009. Drosophila motor axons recognize and
1423 follow a Sidestep-labeled substrate pathway to reach their target fields. *Genes Dev*.
1424 23:1052-1062.
1425 Silbering, A.F., R. Rytz, Y. Grosjean, L. Abuin, P. Ramdya, G.S. Jefferis, and R. Benton. 2011.
1426 Complementary function and integrated wiring of the evolutionarily distinct Drosophila
1427 olfactory subsystems. *J Neurosci*. 31:13357-13375.
1428 Sink, H., E.J. Rehm, L. Richstone, Y.M. Bulls, and C.S. Goodman. 2001. sidestep encodes a target-
1429 derived attractant essential for motor axon guidance in Drosophila. *Cell*. 105:57-67.
1430 Song, E., B. de Bivort, C. Dan, and S. Kunes. 2012. Determinants of the Drosophila odorant
1431 receptor pattern. *Dev Cell*. 22:363-376.
1432 Sweeney, L.B., A. Couto, Y.H. Chou, D. Berdnik, B.J. Dickson, L. Luo, and T. Komiyama. 2007.
1433 Temporal target restriction of olfactory receptor neurons by Semaphorin-1a/PlexinA-
1434 mediated axon-axon interactions. *Neuron*. 53:185-200.
1435 Sweeney, S.T., K. Broadie, J. Keane, H. Niemann, and C.J. O'Kane. 1995. Targeted expression of
1436 tetanus toxin light chain in Drosophila specifically eliminates synaptic transmission and
1437 causes behavioral defects. *Neuron*. 14:341-351.
1438 Tan, L., K.X. Zhang, M.Y. Pecot, S. Nagarkar-Jaiswal, P.T. Lee, S.Y. Takemura, J.M. McEwen, A. Nern,
1439 S. Xu, W. Tadros, Z. Chen, K. Zinn, H.J. Bellen, M. Morey, and S.L. Zipursky. 2015. Ig
1440 Superfamily Ligand and Receptor Pairs Expressed in Synaptic Partners in Drosophila. *Cell*.
1441 163:1756-1769.
1442 Task, D., C.C. Lin, A. Vulpe, A. Afify, S. Ballou, M. Brbic, P. Schlegel, J. Raji, G. Jefferis, H. Li, K.
1443 Menuz, and C.J. Potter. 2022. Chemoreceptor co-expression in Drosophila melanogaster
1444 olfactory neurons. *Elife*. 11.
1445 Tegenfeldt, F., D. Kuznetsov, M. Manni, M. Berkeley, E.M. Zdobnov, and E.V. Kriventseva. 2025.
1446 OrthoDB and BUSCO update: annotation of orthologs with wider sampling of genomes.
1447 *Nucleic Acids Res*. 53:D516-D522.
1448 Tichy, A.L., A. Ray, and J.R. Carlson. 2008. A new Drosophila POU gene, pdm3, acts in odor
1449 receptor expression and axon targeting of olfactory neurons. *J Neurosci*. 28:7121-7129.
1450 Trible, W., L. Olivos-Cisneros, S.K. McKenzie, J. Saragosti, N.C. Chang, B.J. Matthews, P.R. Oxley,
1451 and D.J.C. Kronauer. 2017. orco Mutagenesis Causes Loss of Antennal Lobe Glomeruli and
1452 Impaired Social Behavior in Ants. *Cell*.
1453 Venkatasubramanian, L., Z. Guo, S. Xu, L. Tan, Q. Xiao, S. Nagarkar-Jaiswal, and R.S. Mann. 2019.
1454 Stereotyped terminal axon branching of leg motor neurons mediated by IgSF proteins DIP-
1455 alpha and Dpr10. *Elife*. 8.
1456 Venken, K.J., K.L. Schulze, N.A. Haelterman, H. Pan, Y. He, M. Evans-Holm, J.W. Carlson, R.W.
1457 Levis, A.C. Spradling, R.A. Hoskins, and H.J. Bellen. 2011. MiMIC: a highly versatile

1458 transposon insertion resource for engineering Drosophila melanogaster genes. *Nat*
1459 *Methods*. 8:737-743.
1460 Vien, K.M., Q. Duan, C. Yeung, and P.C. Volkan. 2023. Conserved atypical cadherin, Fat2, regulates
1461 axon terminal organization in the developing Drosophila olfactory sensory neurons.
1462 *bioRxiv*:2023.2007. 2028.550990.
1463 Wang, Y., M. Lobb-Rabe, J. Ashley, P. Chatterjee, V. Anand, H.J. Bellen, O. Kanca, and R.A. Carrillo.
1464 2022. Systematic expression profiling of Dpr and DIP genes reveals cell surface codes in
1465 Drosophila larval motor and sensory neurons. *Development*. 149.
1466 Ward, A., W. Hong, V. Favaloro, and L. Luo. 2015. Toll receptors instruct axon and dendrite
1467 targeting and participate in synaptic partner matching in a Drosophila olfactory circuit.
1468 *Neuron*. 85:1013-1028.
1469 White, B.H., T.P. Osterwalder, K.S. Yoon, W.J. Joiner, M.D. Whim, L.K. Kaczmarek, and H.
1470 Keshishian. 2001. Targeted attenuation of electrical activity in Drosophila using a
1471 genetically modified K(+) channel. *Neuron*. 31:699-711.
1472 Xie, Q., M. Brbic, F. Horns, S.S. Kolluru, R.C. Jones, J. Li, A.R. Reddy, A. Xie, S. Kohani, Z. Li, C.N.
1473 McLaughlin, T. Li, C. Xu, D. Vacek, D.J. Luginbuhl, J. Leskovec, S.R. Quake, L. Luo, and H. Li.
1474 2021. Temporal evolution of single-cell transcriptomes of Drosophila olfactory projection
1475 neurons. *Elife*. 10.
1476 Xie, Q., J. Li, H. Li, N.D. Udeshi, T. Svinkina, D. Orlin, S. Kohani, R. Guajardo, D.R. Mani, C. Xu, T. Li,
1477 S. Han, W. Wei, S.A. Shuster, D.J. Luginbuhl, S.R. Quake, S.E. Murthy, A.Y. Ting, S.A. Carr,
1478 and L. Luo. 2022. Transcription factor Acj6 controls dendrite targeting via a combinatorial
1479 cell-surface code. *Neuron*. 110:2299-2314 e2298.
1480 Xie, Q., B. Wu, J. Li, C. Xu, H. Li, D.J. Luginbuhl, X. Wang, A. Ward, and L. Luo. 2019. Transsynaptic
1481 Fish-lips signaling prevents misconnections between nonsynaptic partner olfactory
1482 neurons. *Proc Natl Acad Sci U S A*. 116:16068-16073.
1483 Xu, C., E. Theisen, R. Maloney, J. Peng, I. Santiago, C. Yapp, Z. Werkhoven, E. Rumbaut, B. Shum,
1484 D. Tarnogorska, J. Borycz, L. Tan, M. Courgeon, T. Griffin, R. Levin, I.A. Meinertzhagen, B. de
1485 Bivort, J. Drugowitsch, and M.Y. Pecot. 2019. Control of Synaptic Specificity by Establishing
1486 a Relative Preference for Synaptic Partners. *Neuron*. 103:865-877 e867.
1487 Xu, S., A.P. Sergeeva, P.S. Katsamba, S. Mannepalli, F. Bahna, J. Bimela, S.L. Zipursky, L. Shapiro,
1488 B. Honig, and K. Zinn. 2022. Affinity requirements for control of synaptic targeting and
1489 neuronal cell survival by heterophilic IgSF cell adhesion molecules. *Cell Rep*. 39:110618.
1490 Xu, S., Q. Xiao, F. Cosmanescu, A.P. Sergeeva, J. Yoo, Y. Lin, P.S. Katsamba, G. Ahlsen, J. Kaufman,
1491 N.T. Linaval, P.T. Lee, H.J. Bellen, L. Shapiro, B. Honig, L. Tan, and S.L. Zipursky. 2018.
1492 Interactions between the Ig-Superfamily Proteins DIP-alpha and Dpr6/10 Regulate
1493 Assembly of Neural Circuits. *Neuron*. 100:1369-1384 e1366.
1494 Yan, H., C. Opachaloemphan, G. Mancini, H. Yang, M. Gallitto, J. Mlejnek, A. Leibholz, K. Haight,
1495 M. Ghaninia, L. Huo, M. Perry, J. Slone, X. Zhou, M. Traficante, C.A. Penick, K. Dolezal, K.
1496 Gokhale, K. Stevens, I. Fetter-Pruneda, R. Bonasio, L.J. Zwiebel, S.L. Berger, J. Liebig, D.
1497 Reinberg, and C. Desplan. 2017. An Engineered orco Mutation Produces Aberrant Social
1498 Behavior and Defective Neural Development in Ants. *Cell*.
1499 Yoo, J., M. Dombrovski, P. Mirshahidi, A. Nern, S.A. LoCascio, S.L. Zipursky, and Y.Z.
1500 Kurmangaliyev. 2023. Brain wiring determinants uncovered by integrating connectomes
1501 and transcriptomes. *Curr Biol*. 33:3998-4005 e3996.

1502 Yu, H.H., C.F. Kao, Y. He, P. Ding, J.C. Kao, and T. Lee. 2010. A complete developmental sequence
1503 of a Drosophila neuronal lineage as revealed by twin-spot MARCM. *PLoS Biol*. 8.
1504 Zhu, H., T. Hummel, J.C. Clemens, D. Berdnik, S.L. Zipursky, and L. Luo. 2006. Dendritic patterning
1505 by Dscam and synaptic partner matching in the Drosophila antennal lobe. *Nat Neurosci*.
1506 9:349-355.
1507 Zhu, H., and L. Luo. 2004. Diverse functions of N-cadherin in dendritic and axonal terminal
1508 arborization of olfactory projection neurons. *Neuron*. 42:63-75.
1509 zur Lage, P.I., D.R. Prentice, E.E. Holohan, and A.P. Jarman. 2003. The Drosophila proneural gene
1510 amos promotes olfactory sensillum formation and suppresses bristle formation.
1511 *Development*. 130:4683-4693.

1512